7

The Stratosphere of Jupiter

J. I. Moses
Lunar and Planetary Institute

T. Fouchet
Oxford University

R. V. Yelle
University of Arizona

A. J. Friedson, G. S. Orton
Jet Propulsion Laboratory, California Institute of Technology

B. Bézard and P. Drossart
Observatoire de Paris, Meudon

G. R. Gladstone
Southwest Research Institute

T. Kostiuk
NASA Goddard Space Flight Center

T. A. Livengood
Challenger Center for Space Science Education

7.1 INTRODUCTION

Atmospheric composition, thermal structure, and dynamics are intimately related. Composition affects the thermal structure through the local absorption of solar radiation and the emission of longer wavelength planetary radiation. Density and thermal gradients affect atmospheric motions, which in turn affect composition and thermal structure by transporting heat and chemical constituents from place to place. Because of this intimate relationship between different atmospheric processes, we have chosen in this chapter to focus on how these processes or properties combine to affect a particular region of Jupiter's atmosphere rather than focusing on one specific atmospheric process. Our main concern here is the stratosphere, an atmospheric region bounded from below by the tropopause temperature-minimum (~100–300 mbar) and from above by the base of the high-temperature thermosphere (~10^{-3} mbar). This division of the atmosphere into specific regions defined by the temperature profile has a physical basis – each region is governed by different physical and chemical processes that relate to the different available energy sources and transport mechanisms. Topics related to the jovian troposphere are covered in Chapter 4, and topics related to the thermosphere are discussed in Chapter 9. We restrict ourselves to gas-phase properties and characteristics; stratospheric hazes are described in Chapter 5.

Radiative processes dominate energy transport in the stratosphere. Stratospheric gases absorb ultraviolet and near-infrared radiation from the Sun and infrared radiation from deeper atmospheric levels; that energy is reradiated at thermal-infrared wavelengths. At typical jovian stratospheric pressures, much of the thermal radiation can escape directly to space, allowing the atmosphere to cool. Jupiter's stratosphere is heated largely through absorption of solar radiation in methane bands at near-infrared wavelengths and is cooled through emissions in vibrational bands of ethane, acetylene, and methane at mid-infrared wavelengths and through collisionally induced transitions of H_2–H_2 and H_2–He at mid to far-infrared wavelengths. Vertical motions are inhibited by large positive temperature gradients in the lower stratosphere that trend to nearly isothermal temperature gradients within the middle and upper stratosphere. Stratospheric transport processes therefore tend to be slow and of broad extent. Composition in Jupiter's stratosphere is affected by disequilibrium processes like photochemistry rather than being controlled solely by thermochemical equilibrium and condensation. Many of the disequilibrium chemical products are long-lived and play a major role in regulat-

ing the thermal structure of the stratosphere. Photochemical products often appear distinctly in spectra of Jupiter at ultraviolet and infrared wavelengths. Because of its remote-sensing accessibility over a broad range of wavelengths and because of its lack of optically thick clouds, the stratosphere is a relatively easy region to probe, and we have more information about the jovian stratosphere than we do about other regions of Jupiter's atmosphere.

In this chapter, we review current knowledge of the important properties and processes that characterize the jovian stratosphere. Inferences from both observations and theory are considered. In Section 7.2, we discuss the observed composition of the jovian stratosphere: what gases are observed to be present, how their presence was determined, how they are distributed throughout the stratosphere, and whether their abundances vary with time. In Section 7.3, we delve into the reasons behind the observed composition. We examine potential sources of the observed constituents and discuss theoretical predictions regarding the distribution, evolution, and behavior of stratospheric gases. The thermal structure and energy balance of the stratosphere are discussed in Section 7.4. We describe how temperatures vary with altitude, latitude, and longitude and discuss the observational evidence and theoretical explanations for vertical and horizontal variations. In Section 7.5, we discuss dynamical motions within the stratosphere and consider the evidence for and our understanding of meridional transport mechanisms.

7.2 OBSERVED COMPOSITION

7.2.1 Hydrogen and Helium

Jupiter's low density – recognized for almost two centuries – has long implied that hydrogen and helium are the dominant planetary constituents. However, both H_2 and He are difficult to observe spectroscopically, and definitive evidence for these constituents and their relative abundances had to await advances in infrared observing technology that developed in the twentieth century. The bulk atmospheric abundance of hydrogen and helium has important implications for the planet's origin and evolution, and the relevant observations are covered in more detail in Chapter 2 and Chapter 4.

Although several observers have attempted to determine the abundance of H_2 above the visible cloud tops (e.g., Stecher 1965, Spinrad and Trafton 1963, Trafton 1967), deriving properties of H_2 in the stratosphere itself is difficult. A recent analysis of the $S(0)$ and $S(1)$ quadrupole lines observed by the Infrared Space Observatory Short-Wavelength Spectrometer shows that the H_2 para fraction is not in thermodynamic equilibrium in the lower stratosphere (Fouchet *et al.* 2002). Atomic hydrogen is best studied through the extremely strong resonance line of Lyman alpha (Lyα) at 1216 Å (e.g., Carlson and Judge 1971, Yung and Strobel 1980). Photochemical models of atomic hydrogen indicate that a column of about 10^{17} H atoms cm^{-2} is expected on Jupiter, almost all of which is above $\sim 10^{-4}$ mbar, the pressure level where methane absorption of Lyα begins in the upper stratosphere (e.g., Yung and Strobel 1980, Gladstone *et al.* 1996). Because observations of Lyα pertain mainly to the thermosphere, this topic is covered more fully in Chapter 9. Our current views regarding the He abundance on Jupiter are based on the *Galileo* entry probe measurements using both mass spectrometry (e.g., Niemann *et al.* 1998) and refractive-index analysis (e.g., von Zahn *et al.* 1998). Both techniques are in close agreement and support a helium mole fraction of 0.136 ± 0.003. With a well-established helium abundance and accurate knowledge of the solar flux, the structure of the jovian upper stratosphere may be fruitfully studied by remote sensing of the He I 584 Å resonance line (e.g., Carlson and Judge 1971, McConnell *et al.* 1981, Vervack *et al.* 1995, Gladstone *et al.* 1995), and this method is discussed further in Section 7.3.1.

7.2.2 Methane

Methane (CH_4) – the most abundant spectroscopically active gas in the jovian stratosphere – plays a major role in instigating atmospheric photochemistry and in controlling radiative transport. Wildt (1932) was the first to identify CH_4 in a jovian spectrum. Methane spectral signatures are found at infrared and visible wavelengths, through the vibration-rotation molecular bands, and in the ultraviolet, through an unresolved continuum that exhibits a steep increase in absorption at wavelengths less than ~145 nm. Visible and near-infrared methane bands are mostly formed in the troposphere. In this region, the CH_4 mole fraction is constant because turbulent motions keep the troposphere (and much of the stratosphere) well mixed, because temperatures are high enough that CH_4 never condenses on Jupiter, and because considerable thermochemical conversion to CO occurs only at unaccessibly deep atmospheric levels. Therefore, the mole fraction determined by tropospheric remote-sensing observations and in situ measurements holds for much of the observable portion of Jupiter's atmosphere.

From an analysis of *Voyager* Infrared Interferometric Spectrometer (IRIS) data, Gautier *et al.* (1982) obtain an inferred tropospheric $[CH_4]/[H_2]$ ratio of $(1.95 \pm 0.22) \times 10^{-3}$ for an assumed H_2 mole fraction of 0.897, implying a CH_4 mole fraction of $(1.75 \pm 0.20) \times 10^{-3}$. From *Galileo* Probe Mass Spectrometer data, Niemann *et al.* (1998) derive a CH_4 mole fraction of $(1.81 \pm 0.34) \times 10^{-3}$. These values are consistent to within their respective error bars, and a CH_4 mole fraction of $\sim 1.8 \times 10^{-3}$ should hold true throughout much of the stratosphere. Nevertheless, the methane mole fraction decreases in the upper stratosphere (see Section 7.3.1) due to the growing influence of molecular diffusion at low pressures. Although photochemical destruction of methane also occurs in the upper stratosphere, the contribution of photochemistry to the rapid decrease in the methane mole fraction with altitude is minor compared with the effects of molecular diffusion (e.g., Gladstone *et al.* 1996). Obtaining reliable information about the altitude variation of methane in the upper stratosphere is of major importance to our understanding of stratospheric photochemistry, radiative balance, and atmospheric mixing.

Infrared signatures for stratospheric methane are observed mainly as emission in the ν_4 band at 1307 cm^{-1} (7.8 μm), which can be observed from ground-based telescopes despite the difficulty of observing through the Earth's atmosphere. Gillett *et al.* (1969) reported the first such detection. The ν_4 band has also been observed from space with *Voyager* IRIS (e.g., Hanel *et al.* 1979b,a), with the Infrared Space Observatory Short-Wavelength Spectrometer

(ISO–SWS) (e.g., Encrenaz *et al.* 1996), and now with the Composite Infrared Spectrometer (CIRS) aboard *Cassini* (e.g., Flasar *et al.* 2001). The ν_4 band predominantly probes the lower stratosphere and upper troposphere at pressures greater than $\sim$1 mbar.

Information about the methane abundance in the upper stratosphere of Jupiter can be obtained from observations made at ultraviolet wavelengths. The occultation of the star α Leo as observed in the 51–169 nm range by the Ultraviolet Spectrometer (UVS) experiment on board *Voyager* provided a direct determination of atmospheric absorption by CH_4 and other hydrocarbons (Broadfoot *et al.* 1981, Festou *et al.* 1981, Atreya *et al.* 1981, Yelle *et al.* 1996). However, very different results concerning the upper-stratospheric methane mole fraction have been derived from different analyses of the UVS data set (cf. Festou *et al.* 1981 and Yelle *et al.* 1996). The inversion of the CH_4 mole fraction is highly sensitive to the upper-boundary condition for the temperature of the thermosphere, a region above that sounded by the CH_4 absorption. Festou *et al.* (1981) assumed that the temperatures increased relatively slowly with increasing altitude in the thermosphere, and they derived a CH_4 mole fraction of $2.5^{+3}_{-2} \times 10^{-5}$ at $\sim 5 \times 10^{-3}$ mbar. By using more recent thermospheric temperature measurements and assuming a steeper thermal gradient, Yelle *et al.* (1996) obtained a CH_4 mole fraction of $(1.5 \pm 0.5) \times 10^{-4}$ at $\sim 2 \times 10^{-4}$ mbar.

Two new, promising techniques involving infrared observations have also been used to infer the abundance of methane near the homopause region in Jupiter's upper stratosphere: observations of CH_4 fluorescence at 3.3 μm and observations of methane absorption during stellar occultations. Drossart *et al.* (1999) use ISO–SWS observations of CH_4 fluorescence in the ν_3 band at 3.3 μm to infer a mole fraction of $\sim 5.1 \times 10^{-4}$ near 10^{-3} mbar. Their inferred methane profile is consistent with the UVS occultation analysis of Yelle *et al.* (1996). More recent spatially resolved observations of CH_4 fluorescence emission in the hot band $\nu_3+\nu_4-\nu_4$ obtained with the VLT/ISAAC instrument (Drossart *et al.* 2001) demonstrate that this mole fraction is constant to within ±20% across the jovian disk. Spectroscopic observations of methane absorption in the 2.3 μm methane band, as recorded during the occultation of star HIP9369 by Jupiter in October 1999 (Drossart *et al.* 2000), have also been used to constrain the CH_4 mole fraction in the homopause region; preliminary results are consistent with a methane homopause location in the $\sim 10^{-3}$-mbar range.

The ultraviolet flux from equatorial dayglow and auroral emissions on Jupiter can provide information about upper-stratospheric methane abundances, but only after complex modeling of the H and H_2 radiative transfer is taken into account (e.g., Yung *et al.* 1982, Wagener *et al.* 1985, Livengood *et al.* 1990, Feldman *et al.* 1993, Trafton *et al.* 1994, Liu and Dalgarno 1996b, Ajello *et al.* 1998). Although these observations seldom provide specific information about the methane mole fraction as a function of pressure, they do provide important information about the homopause location and/or the altitude of auroral deposition. From an analysis of 83–185 nm dayglow observations from the Hopkins Ultraviolet Telescope, Liu and Dalgarno (1996b) find slightly less CH_4 absorption than is indicated from auroral-region spectra obtained with the Goddard High Resolution Spectrograph aboard the Hubble Space Telescope (HST) (Trafton *et al.* 1994), implying only minor differences in the homopause levels between the auroral regions and the rest of the planet. This observation is somewhat at odds with recent theoretical modeling of the auroral atmosphere by Grodent *et al.* (2001), who conclude that an increase in the eddy diffusion coefficient and hence the homopause altitude is possible in the auroral regions as compared with equatorial regions.

7.2.3 Ethane and Acetylene

The most abundant and thermally important products of methane photolysis in the jovian stratosphere are ethane (C_2H_6) and acetylene (C_2H_2). These two molecules were first detected on Jupiter by Ridgway (1974), through ground-based thermal-infrared observations of the ν_9 band of C_2H_6 at 822 cm^{-1} and the ν_5 band of C_2H_2 at 729 cm^{-1}. The detections were confirmed by Combes *et al.* (1974). The mole fractions determined from these early studies (Table 7.1) were hampered by low spectral resolution, poor data quality, lack of detailed spectroscopic parameters, and large uncertainties in the stratospheric temperature profile. Later Earth-based observers (e.g., Tokunaga *et al.* 1976, Orton and Aumann 1977) obtained improved C_2H_6 and C_2H_2 mole fractions using newer and more reliable spectroscopic parameters. However, the temperature profile remained poorly constrained, with uncertainties of 17 K at 10 mbar (e.g., Orton 1977). These temperature uncertainties resulted in hydrocarbon abundances that were uncertain by a factor of three.

The *Voyager 1* and *2* Jupiter flybys in 1979 provided extensive information on this issue. The combination of the radio occultation profiles (Lindal *et al.* 1981), the UVS solar occultation profile (Festou *et al.* 1981), and the IRIS spectra of CH_4 emission in its ν_4 band at 1307 cm^{-1} (Hanel *et al.* 1979b,a) sharpened drastically our knowledge of the stratospheric thermal structure from 100 mbar to $\sim$1μbar. Subsequent hydrocarbon observations were analyzed using profiles that matched the radio occultation measurements and best-reproduced selections of *Voyager* IRIS CH_4 spectra for latitudes comparable to those of the observations. Using this information to interpret ground-based observations, and assuming vertically homogeneous abundances, Noll *et al.* (1986) and Kostiuk *et al.* (1987) determined the possible ethane mole fraction at the equator to be between 1.8×10^{-6} and 3.8×10^{-6}. For acetylene, observations obtained by Drossart *et al.* (1986) and Noll *et al.* (1986) led to $[C_2H_2]/[H_2]$ ratios at the equator in the range $(1.0–4.0) \times 10^{-8}$.

Photochemical models predict that the ethane and acetylene mole fractions vary with altitude. This vertical inhomogeneity raises many questions about the previous infrared measurements. What pressure levels do the observations actually probe? How does the assumed vertical distribution affect the published results? Can the real vertical distribution be determined from observations? Kostiuk *et al.* (1987) show that their ability to fully resolve individual lines within the C_2H_6 ν_9 band allows them to probe a broad pressure range within $\sim$0.4–10 mbar, centered at 2 mbar. Although their results were not very sensitive to the assumed mole-fraction distribution, Kostiuk *et al.* (1987) found that a mole fraction change from 2×10^{-6} at 10 mbar

Table 7.1. Ethane and acetylene abundance measurements in non-auroral regions on Jupiter.

Species	Mole fraction	Pressure (mbar)	Latitude	Date	Technique	Reference
C_2H_6	3×10^{-4}		±10°	06/73	IR FTS	Ridgway (1974)
	2×10^{-5}		global ave.	08/73	IR FTS	Combes *et al.* (1974)
	2.6×10^{-5}			04/75	IR FTS	Tokunaga *et al.* (1976)
	2.5×10^{-6}	5×10^{-3}	+16.5°	07/79	UVS	Festou *et al.* (1981)
	6.6×10^{-6}	4	±30°	12/78 & 06/79	IUE	Gladstone and Yung (1983)
	2.6×10^{-6}	5	±8°	06/80	IR FP	Noll *et al.* (1986)
	2.8×10^{-6}	0.4–10	±5°	1982–1983	IR heterodyne	Kostiuk *et al.* (1987)
	4.7×10^{-6}	0.4–10	30–50°N	04/82	IR heterodyne	Kostiuk *et al.* (1987)
	2.6×10^{-6}	0.4–10	30–50°S	04/82	IR heterodyne	Kostiuk *et al.* (1987)
	1.7×10^{-6}	4	±30°	1980–1988	IUE	McGrath *et al.* (1989)
	3.6×10^{-6}	0.3–3	45–55°N	12/89	IR heterodyne	Livengood *et al.* (1993)
	3×10^{-6}	4	±15°	12/90 & 03/95	UV *Astro-1 & 2*	Morrissey *et al.* (1995)
	3.9×10^{-6}	5	global ave.	12/94 & 02/95	IRGS	Sada *et al.* (1998)
	8.6×10^{-6}	1	±30°	05/97	ISO-SWS	Fouchet *et al.* (2000)
	2.2×10^{-6}	10	±30°	05/97	ISO-SWS	Fouchet *et al.* (2000)
	4.6×10^{-6}	0.4–10	−21°	05/97	IRGS	Yelle *et al.* (2001)
C_2H_2	7×10^{-5}		±10°	06/73	IR FTS	Ridgway (1974)
	3×10^{-6}		global ave.	08/73	IR FTS	Combes *et al.* (1974)
	$<6.5 \times 10^{-8}$			04/75	IR FTS	Tokunaga *et al.* (1976)
	1.4×10^{-8}	10^{-1}	global ave.	10/75	IR FTS (KAO)	Orton and Aumann (1977)
	1.9×10^{-8}	10	±30°	01/79 & 04/79	IUE	Owen *et al.* (1980)
	1.0×10^{-7}	10	±30°	1978–1980	IUE	Clarke *et al.* (1982)
	1.0×10^{-7}	10	±30°	12/78 & 06/79	IUE	Gladstone and Yung (1983)
	3×10^{-8}	30	±30°	1978–1980	IUE	Wagener *et al.* (1985)
	8.6×10^{-9}		±3°	07/85	IR FP	Drossart *et al.* (1986)
	3.4×10^{-8}	3	±8°	06/80	IR FP	Noll *et al.* (1986)
	3.55×10^{-8}	10	±30°	1980–1988	IUE	McGrath *et al.* (1989)
	4×10^{-6}	0.1	10–36°S	01/91	IRGS	Bézard *et al.* (1995)
	1×10^{-7}	1	10–36°S	01/91	IRGS	Bézard *et al.* (1995)
	1×10^{-9}	10	10–36°S	01/91	IRGS	Bézard *et al.* (1995)
	3.9×10^{-8}	10	±15°	12/90	UV *Astro-1*	Morrissey *et al.* (1995)
	2.8×10^{-8}	10	±15°	03/95	UV *Astro-2*	Morrissey *et al.* (1995)
	2×10^{-8}	80	6–25°N	05/92	UV HST-FOS	Edgington *et al.* (1998)
	2.3×10^{-8}	8	global ave.	12/94 & 02/95	IRGS	Sada *et al.* (1998)
	4.0×10^{-8}	10	0°	06/93	UV HST-FOS	Bétremieux and Yelle (1999)
	1.5×10^{-8}	20–60	0°	06/93	UV HST-FOS	Bétremieux and Yelle (1999)
	4.8×10^{-7}	0.3	±40°	05/97	ISO-SWS	Fouchet *et al.* (2000)
	3.6×10^{-8}	4	±40°	05/97	ISO-SWS	Fouchet *et al.* (2000)
	2.7×10^{-6}	0.01	+2°	05/97	IRGS	Yelle *et al.* (2001)

Note: When published abundances are provided as the species concentration divided by the concentration of H_2, these ratios have been converted to mole fractions by using the *Galileo* determination of the H_2 mole fraction = 0.8622. Mole fraction values for Noll *et al.* (1986) are for the revised flux calibration given in their Table I. Acetylene mole fractions quoted by Fouchet *et al.* (2000) have been corrected for a computer coding error.

to 3.5×10^{-6} at 1 mbar provided the best fit to their fully resolved line profile. Noll *et al.* (1986) fitted their C_2H_2 and C_2H_6 observations with homogeneous distributions as well as with profiles derived from a photochemical model. Inspection of their results shows that their ethane measurements pertain to a pressure of ~5 mbar (similar to that of Kostiuk *et al.* 1987), while their acetylene measurements pertain to ~3 mbar. Drossart *et al.* (1986) did not estimate the altitudes probed by their C_2H_2 measurement, and it is difficult to determine whether these combined infrared measurements provide any evidence for significant hydrocarbon vertical inhomogeneity.

Ultraviolet observations have also been used to infer the ethane and acetylene abundances in the jovian stratosphere. Results obtained from ultraviolet observations have the advantage of being far less sensitive to the temperature profile than results from infrared observations. As a drawback, the blending of many featureless absorption cross sections due to several chemical species or aerosols and the potential sensitivity of the results to aerosol-extinction modeling strongly limit the effectiveness of ultraviolet observations. In fact, acetylene is the only stratospheric molecule that is unambiguously detected in Jupiter's ultraviolet spectrum through its characteristic $\tilde{X}^1\Sigma_g^+ \rightarrow \tilde{A}^1A_u$ and $\tilde{X}^1\Sigma_g^+ \rightarrow \tilde{B}^1B_u$ transitions. Acetylene also exhibits some very strong narrow peaks at 144, 148, and 152 nm (e.g., Smith *et al.* 1991) that can be useful in identifying this molecule in ultraviolet spectra (e.g., through absorption in spectra from the auroral regions; see Clarke *et al.* 2000, Dols *et al.* 2000) or during ultraviolet occultations. In contrast, as stated by Morrissey *et al.* (1995), "the presence of ethane is indicated by a significantly better fit to the data than is found with either methane or propane."

Owen *et al.* (1980) first identified C_2H_2 signatures in

the jovian ultraviolet spectrum from data obtained with the IUE. They inferred the $[C_2H_2]/[H_2]$ ratio to be 2.2×10^{-8} (assuming C_2H_2 to be well-mixed throughout the stratosphere). Clarke *et al.* (1982), Gladstone and Yung (1983), Wagener *et al.* (1985), and McGrath *et al.* (1989) also used IUE data to determine a C_2H_2 mole fraction of $(1.0 \pm 0.5) \times 10^{-7}$, $(1.0 \pm 0.1) \times 10^{-7}$, $(3 \pm 1) \times 10^{-8}$, and 3.6×10^{-8}, respectively. More recently Jupiter was observed with the Hopkins Ultraviolet Telescope (HUT) during its *Astro-1* and *Astro-2* flights (Morrissey *et al.* 1995), and with the Faint Object Spectrograph (FOS) onboard HST (Edgington *et al.* 1998). These three observations gave very similar C_2H_2 mole fractions of respectively: $(3.9 \pm 0.3) \times 10^{-8}$, $(2.8 \pm 0.3) \times 10^{-8}$, and $(2 \pm 1) \times 10^{-8}$. Bétremieux and Yelle (1999) analyzed HST Goddard High Resolution Spectrograph observations of the jovian equatorial atmosphere in the 170–230 nm region using a model that included Raman scattering of ultraviolet radiation and allowed a cleaner separation of Rayleigh and aerosol scattering processes than was previously possible. These authors derived C_2H_2 mole fractions of 4×10^{-8} at 0–20 mbar, 1.5×10^{-8} at 20–60 mbar, 4×10^{-8} at 60–80 mbar, 8×10^{-8} at 80–120 mbar, and 1.5×10^{-7} at >120 mbar; however, the results for pressures greater than ~60 mbar are in conflict with the line shapes observed at thermal infrared wavelengths. For ethane, Gladstone and Yung (1983), McGrath *et al.* (1989), and Morrissey *et al.* (1995) respectively found mole fractions of $(6.6 \pm 5.3) \times 10^{-6}$, 1.7×10^{-6}, and $(2.9^{+1.0}_{-0.8}) \times 10^{-6}$ (*Astro-1*) and $(3.0^{+0.8}_{-0.6}) \times 10^{-6}$ (*Astro-2*).

The C_2H_2 mole fraction of $\sim 1 \times 10^{-7}$ inferred by Gladstone and Yung (1983) and Clarke *et al.* (1982) does not agree with the results obtained from other ultraviolet measurements that cluster around $\sim 3 \times 10^{-8}$. However, we note that the depth reached by UV photons in the atmosphere strongly depends on their wavelength, with shorter wavelengths probing higher altitudes or lower pressures. This wavelength dependence suggests that the Gladstone and Yung (1983) results are not inconsistent with other ultraviolet studies, but rather that Gladstone and Yung probe higher altitudes than the other authors. Gladstone and Yung restricted themselves to the 150–175 nm wavelength interval that sounds pressure levels above the 1- to 10-mbar level, while other studies made use of longer wavelengths that probe down below the 10-mbar level. Similarly, the C_2H_2 mole fraction of $\sim 1 \times 10^{-7}$ from Clarke *et al.* (1982) was derived from an analysis of the C_2H_2 absorption band depths near 170 nm; Clarke *et al.* show that mole fractions of 2×10^{-8} would produce C_2H_2 absorption bands that are too shallow in this wavelength region. The apparent discrepancy between the results of Clarke *et al.* (1982) and Gladstone and Yung (1983) and those of later investigators may therefore be viewed as evidence that the C_2H_2 mole fraction increases with altitude (see also Yelle *et al.* 2001).

Bézard *et al.* (1995) first demonstrated from infrared spectroscopy that the C_2H_2 mole fraction increases with height in the stratosphere. Their profile, adjusted to fit some strong ν_5 lines and some weak $\nu_4+\nu_5-\nu_4$ lines observed at high spectral resolution, has mole fractions of 4×10^{-6}, 1×10^{-7} and 1×10^{-9} at 0.1, 1 and 10 mbar respectively. Fouchet *et al.* (2000) used the entire ν_5 and $\nu_4+\nu_5-\nu_4$ bands observed by ISO–SWS to confirm the drop in acetylene with increasing pressure. Their derived $[C_2H_2]/[H_2]$ ratios,

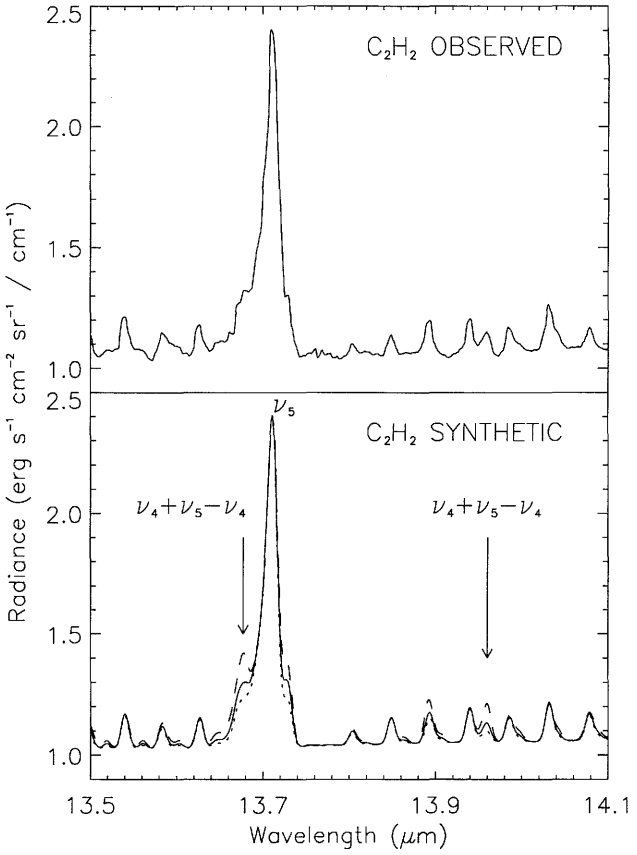

Figure 7.1. The ISO–SWS spectrum of Jupiter from the 13.5–14.1 μm region (top panel) compared with synthetic spectra (bottom panel) calculated for different vertical distributions of C_2H_2 (from Fouchet *et al.* 2000). A mole fraction gradient of $\mathrm{d}\ln q/\mathrm{d}\ln P \approx -0.9$ in the 0.3–10 mbar region (solid line) best reproduces the observations.

$(5.6^{+1.0}_{-0.5}) \times 10^{-7}$ at 0.3 mbar and $(4.2^{+0.7}_{-0.4}) \times 10^{-8}$ at 4 mbar, agree well with the Bézard *et al.* (1995) results. Figure 7.1 shows the ISO emission spectra from the C_2H_2 ν_5 band region (from Fouchet *et al.* 2000). From observations of the R(5) emission line of the ν_5 band, Sada *et al.* (1998) inferred a mole fraction of $(2.3 \pm 0.5) \times 10^{-8}$ at 8 mbar using a height-dependent vertical distribution. Yelle *et al.* (2001) also tested different possible vertical distributions against their ground-based observations of one C_2H_2 ν_5 line. They found that by adopting the values derived by Wagener *et al.* (1985) and Fouchet *et al.* (2000) for the C_2H_2 mole fraction between 10 and 0.3 mbar, the acetylene mole fraction at 0.01 mbar is then constrained to lie between $(1.1\text{–}4.3) \times 10^{-6}$. All of these studies draw a consistent picture of the acetylene mole fraction q decreasing with increasing pressure P with a gradient of $\mathrm{d}\ln q/\mathrm{d}\ln P = -0.9 \pm 0.2$ in the jovian stratosphere.

The ethane mole fraction is expected to vary less rapidly with altitude than acetylene. No evidence of vertical variation is seen in comparisons between C_2H_6 measurements in the ultraviolet, especially between the UVS occultation value of $(2.5^{+2.0}_{-1.5}) \times 10^{-6}$ (Festou *et al.* 1981), which pertains to 5 μbar, and other ultraviolet measurements that probe higher pressures (~4 mbar) and that cluster around 3×10^{-6} (Gladstone and Yung 1983, McGrath *et al.* 1989,

Morrissey *et al.* 1995). The ISO–SWS spectrometer recorded the ν_9 band of ethane in a single exposure with a resolving power of $R \sim 1500$. Testing different C_2H_6 vertical distributions against this dataset, Fouchet *et al.* (2000) were able to retrieve the ethane abundance at two different pressure levels, 1 mbar and 10 mbar, where the $[C_2H_6]/[H_2]$ ratios were inferred to be $(1.0 \pm 0.2) \times 10^{-5}$ and $2.6^{+0.5}_{-0.6} \times 10^{-6}$, respectively. Fouchet *et al.* (2000) constrained the slope of the C_2H_6 mole-fraction distribution to be $\mathrm{d}\ln q/\mathrm{d}\ln P = -0.6 \pm 0.2$ in the lower stratosphere. This result is consistent with the analyses of Kostiuk *et al.* (1987), Sada *et al.* (1998), and Yelle *et al.* (2001). The latter two groups analyzed their data using height-dependent ethane profiles and reported mole fractions of $(3.9^{+1.9}_{-1.3}) \times 10^{-6}$ at 5 mbar (Sada *et al.* 1998) and $(2.8\text{–}6.5) \times 10^{-6}$ at 0.4–10 mbar (Yelle *et al.* 2001).

7.2.4 Other Hydrocarbons

Many hydrocarbons possess strong absorption bands in the ultraviolet and thermal infrared, and both spectral regions have been widely used to search for new species. In the ultraviolet, however, many of the absorption bands look similar because they are without characteristic features; therefore, authors have reported only tentative detections from the UV range. The analysis of thermal infrared spectra, where vibrational bands occur at positions uniquely assigned to each molecule, has been much more fruitful. Thermal infrared observations of Jupiter's polar regions have been of particular interest for the detection of minor species because the conjunction of a temperature enhancement and possible abundance enhancement due to auroral precipitation induces more prominent emission features.

Authors have interpreted their observations either with vertically uniform mole fractions or with vertical distributions obtained from photochemical models. In order to compare the various works presented below, we have converted the numerical results into column density above the 50-mbar pressure level. This approach is based on the fact that infrared lines are optically thin for minor hydrocarbons and that ultraviolet observations approximately probe the atmosphere down to the 50-mbar level. The vertical distribution profile and the temperature profile adopted to analyze a set of observations also strongly influence the inferred abundances, especially in the auroral regions where a large temperature enhancement exists in the upper stratosphere, as is attested by enhanced emission in the methane ν_4 band and hydrocarbon bands (see Section 7.4.1 and Section 7.2.7). As both profiles are still uncertain, values derived at the equator and polar regions should be compared only with caution.

C species. Methyl radicals (CH_3) were detected in the north auroral region by CIRS at the occasion of the *Cassini* Jupiter flyby (Jennings *et al.* 2001). No inferred abundance is available at this time.

C_2 species. Ethylene (C_2H_4) is the least abundant of the stable C_2H_x photochemical products, with an expected abundance of respectively ten times less and a thousand times less than acetylene and ethane. Ethylene had thus eluded detection up to the analysis of *Voyager* IRIS north polar spectra by Kim *et al.* (1985). These authors modeled the ν_7 band of C_2H_4 at 949 cm^{-1} and retrieved a column density of $(3.4 \pm 1.5) \times 10^{16}$ molecules cm^{-2} for a uniform $[C_2H_4]/[H_2]$ ratio of $(7 \pm 3) \times 10^{-9}$. Their measurement pertains to an approximate latitude of 60° N within the projected auroral region and assumes a temperature profile such that the middle and upper stratosphere is ~185 K. Kostiuk *et al.* (1989) and Kostiuk *et al.* (1993) first claimed C_2H_4 detection at Jupiter's equator from infrared heterodyne ground-based spectroscopy with resolving power $\sim 10^6$. Adopting a vertical profile obtained from photochemical models and using molecular parameters available at the time, they derived a column abundance of 1.2×10^{16} cm^{-2}. This value is greater than the upper limits at the equator inferred from analyses of Jupiter's ultraviolet spectrum: Gladstone and Yung (1983) established a limiting column density of 4.4×10^{15} cm^{-2}, while Wagener *et al.* (1985) and Morrissey *et al.* (1995) decreased this limit respectively to 4.0×10^{15} and 2.2×10^{15} cm^{-2}. More recently, Bézard *et al.* (2001b) detected several lines of the C_2H_4 ν_7 band at Jupiter's equator and retrieved a column abundance of 6×10^{14} cm^{-2}, a value consistent with the upper limits derived from ultraviolet observations. Note that after taking into account differences in the spectral resolution and viewing geometry, the Bézard *et al.* line intensities are about an order of magnitude weaker than what the Kostiuk *et al.* (1989) and Kostiuk *et al.* (1993) observations would imply. Thus, the two sets of infrared observations, rather than merely the data analysis techniques, are in disagreement.

C_3 species. Methylacetylene (CH_3C_2H) was first detected in the polar region by Kim *et al.* (1985), who found a column density of $1.2^{+1.0}_{-0.5} \times 10^{16}$ molecules cm^{-2} (uniform $[CH_3C_2H]/[H_2]$ ratio of $2.5^{+2}_{-1} \times 10^{-9}$). Kim *et al.* (1985) also inferred an upper limit of 3.4×10^{15} molecules cm^{-2} ($[CH_3C_2H]/[H_2] = 7 \times 10^{-10}$) at the equator, a value that superseded the limit of 1.1×10^{16} cm^{-2} determined by Wagener *et al.* (1985). The high signal-to-noise ratio achieved by the ISO–SWS instrument allowed Fouchet *et al.* (2000) to detect CH_3C_2H at the jovian equator and to retrieve a column density of $(1.5 \pm 0.4) \times 10^{15}$ cm^{-2}.

Wagener *et al.* (1985) tentatively detected allene (CH_2CCH_2) in the ultraviolet spectrum. They found that a column density of $(3.8 \pm 2.2) \times 10^{15}$ cm^{-2} (a uniform mole fraction of $(7 \pm 4) \times 10^{-10}$) best fitted Jupiter's IUE spectrum. Wagener *et al.* (1985) have checked that this value is consistent with the upper limit, 3.4×10^{16} cm^{-2} (6×10^{-9}), that can be derived from the IRIS spectra at the equator.

Propane (C_3H_8) has not been detected in the thermal infrared. The upper limit in the auroral zone is set to 2.9×10^{18} cm^{-2} by Kim *et al.* (1985), while Wagener *et al.* (1985) established a much more stringent limit of 8.4×10^{16} cm^{-2} at the equator of the planet. From observations of an energetic and unusually deep-penetrating auroral storm on Jupiter, Clarke *et al.* (2000) report evidence for overlying absorption by CH_3C_2H and C_3H_8 in their HST/STIS ultraviolet spectra; although the identification is not definitive, the model-data fit is greatly improved by the inclusion of these species.

C_4 species. Gladstone and Yung (1983) found that the presence of diacetylene (C_4H_2) with a column density of $(1.6 \pm 1.1) \times 10^{15}$ cm^{-2}, corresponding to a uniform mole fraction of $(2.9 \pm 2) \times 10^{-10}$, was necessary to obtain a good fit of their IUE data. However, they did not claim any detection since other absorbers could have the same effect on the spectrum. The first attempts to detect diacetylene in the

thermal infrared were also unsuccessful. Kim *et al.* (1985) put an upper limit of $(1.4 \pm 1.0) \times 10^{15}$ cm^{-2} ($[C_4H_2]/[H_2] = 3 \times 10^{-10}$) in the north polar zone, while Fouchet *et al.* (2000) decreased the upper limit to 7×10^{13} cm^{-2} in the equatorial region. However, C_4H_2 was detected by CIRS (Jennings *et al.* 2001) in the north polar zone at the occasion of the *Cassini* Jupiter flyby. No abundance has yet been inferred from these observations. Clarke *et al.* (2000) report evidence for the presence of both C_4H_2 and C_4H_{10} (butane) in HST/STIS ultraviolet spectra of a deep, energetic auroral storm; inferred abundances are not yet available.

C_6 species. Kim *et al.* (1985) first detected benzene (C_6H_6) emission at 674 cm^{-1} (ν_4 band) in the IRIS spectra in the north polar region. This detection was extended to the entire planet and especially to regions outside the north and south auroral regions by Bézard *et al.* (2001a) from ISO–SWS observations. Using a vertically uniform mole fraction, Kim *et al.* (1985) derived a column abundance of $9.7^{+9.7}_{-4.8} \times 10^{15}$ molecules cm^{-2} $[C_6H_6]/[H_2]$ ratio of $2^{+2}_{-1} \times 10^{-9}$). As the benzene vertical distribution has not yet been accurately modeled, Bézard *et al.* (2001a) analyzed the ISO–SWS spectra with profiles showing the same vertical dependence as modeled for other species (CH_3, C_2H_6 or C_2H_2) and inferred a column density in non-auroral regions of $9^{+4.5}_{-7.5} \times 10^{14}$ cm^{-2}. Bézard *et al.* (2001a) noted that ISO–SWS spectra over the poles showed an increased C_6H_6 emission compared to the spectrum over the equatorial and tropical regions; such behavior is not observed for C_2H_2 emission at the low ISO spatial resolution. They argued that this different behavior can be attributed either to an enhanced C_6H_6 abundance over the pole or to a steeper vertical profile for C_6H_6.

7.2.5 Oxygen Compounds

Jovian carbon monoxide (CO) was first detected by Beer (1975) in the 4.7-μm window, and since then the vertical distribution of this compound, and accordingly its origin, have remained controversial topics (e.g., Beer and Taylor 1998, Noll and Knacke 1998). In a follow-up to the original detection, Beer and Taylor (1978) observed Jupiter at the positions of eighteen lines of the (1–0) band of CO and, from the relative intensities of the absorption features, derived a column density of $(4^{+4}_{-2}) \times 10^{17}$ molecules cm^{-2} at a rotational temperature of 100–150 K. From this relatively low temperature, they suggested that CO is non-uniformly mixed and concentrated in the stratosphere. They also excluded mole fractions in the troposphere larger than a few 1×10^{-10}. Doing the same analysis with 0.5-cm^{-1} resolution spectra recorded with the Kuiper Airborne Observatory, Larson *et al.* (1978) derived a larger rotational temperature, 150–300 K, at odds with the conclusions from Beer and Taylor (1978). These early studies clearly suffered from limitations in the available spectroscopic databases, as most CO lines are blended with those from other absorbers. Bjoraker *et al.* (1986) presented a reanalysis of the Larson *et al.* (1978) spectra. Utilizing improved linelists and radiative transfer calculations, they concluded that a tropospheric, well-mixed distribution with a mole fraction of $(1 \pm 0.2) \times 10^{-9}$ provides a better fit to most observed features than do stratospheric profiles.

Noll *et al.* (1988) tried to resolve the controversy by recording six CO lines at a much higher spectral resolution, 0.07 cm^{-1}, using the Fabry–Perot spectrometer at UKIRT. They found that these lines had broad absorption wings and concluded that carbon monoxide was uniformly mixed with a mole fraction of $(1.6 \pm 0.3) \times 10^{-9}$. Large quantities of CO at altitudes above the ~1-bar level would have produced unresolved absorption cores which are not present in these data. More recently, Noll *et al.* (1997) observed the R5 and R7 CO lines at a similar spectral resolution (0.11 cm^{-1}). They found that, besides broad wings, these lines also exhibited narrow cores that require enhanced concentrations in the upper troposphere/stratosphere (typically 1×10^{-7} at $p < 200$ mbar) compared with the 1.3×10^{-9} mole fraction inferred in the lower troposphere. These data actually contradict those presented by Noll *et al.* (1988), and the reason for this disagreement remains mysterious (Noll and Knacke 1998).

Bézard *et al.* (2002) improved on existing data by observing thirteen CO lines near 4.7 μm in a 5-μm hot-spot region on Jupiter with the FTS spectrometer at CFHT at an unprecedented resolution of 0.045 cm^{-1}. From a radiative transfer analysis, they concluded that the CO mole fraction is $(1 \pm 0.2) \times 10^{-9}$ around ~6 bar and that the mole fraction is larger at higher altitudes in the upper troposphere/stratosphere. This analysis supports the Noll *et al.* (1997) inference of an increasing-with-height profile, but the stratospheric enhancement derived by Bézard *et al.* is ~40 times smaller. Using various test profiles, Bézard *et al.* derived a column abundance above the 0.5-bar level of (8–13) $\times 10^{16}$ molecules cm^{-2} in addition to the amount deposited by the comet Shoemaker–Levy 9 (SL9) collision in 1994 (e.g., Lellouch *et al.* 1997, Moreno 1998). The column abundance provided by an external source alone (non-SL9) was estimated to be $4^{+3}_{-2} \times 10^{16}$ molecules cm^{-2}, while the $\sim 1 \times 10^{-9}$ tropospheric mole fraction requires an internal source.

Water vapor (H_2O) was detected in the upper atmospheres of the four giant planets by ISO (Feuchtgruber *et al.* 1997, 1999). In 1997, five rotational lines at 39.38, 40.33, 43.89 and 44.19 μm were observed on Jupiter by ISO–SWS at a resolving power of 31 000. A disk-averaged column density of (0.8–2.2) $\times 10^{15}$ molecules cm^{-2} was inferred from a preliminary analysis of these observations (Feuchtgruber *et al.* 1999). In November 1997, two other H_2O rotational lines were detected at longer wavelengths (66.44 and 99.49 μm) by the Long-Wavelength Spectrometer (LWS) of ISO at a resolution of approximately 9000 (Lellouch *et al.* 2002). More recently, the Submillimeter Wave Astronomy Satellite (SWAS) detected the 557-GHz (538.3 μm) H_2O line with a resolving power ~3×10^5 (Bergin *et al.* 2000). From the spectrally resolved profile of the line, the authors showed that H_2O is not uniformly mixed above the expected condensation level (~10 mbar) but instead increases with height. They derived a total H_2O column density of about 3×10^{15} molecules cm^{-2}, 1.5–2.5 times larger than inferred from ISO. Note that for all these H_2O observations, the instrumental aperture covers all jovian latitudes so that no spatial resolution is accessible. Reanalyzing the whole set of H_2O observations, Lellouch *et al.* (2002) showed that reproducing simultaneously the LWS and SWS lines requires that water vapor is concentrated high in the atmosphere, above the 0.3–

0.7 mbar level, with a column density of $(2.0 \pm 0.5) \times 10^{15}$ molecules cm^{-2} and concluded that the observed water is probably residual from the SL9 impacts. Such a model, however, slightly underestimates the SWAS line intensity, possibly because of uncertainties in the baseline of these heterodyne measurements. The retrieved column density is consistent with the non-detection of water vapor in ultraviolet spectra (Wagener *et al.* 1985). Analyzing spectra recorded by IUE, Wagener *et al.* inferred an upper limit on the mean H_2O mole fraction in the 0–100 mbar region equal to 2×10^{-8}, corresponding to a stratospheric abundance of less than 2×10^{17} molecules cm^{-2}.

Carbon dioxide (CO_2) was detected by ISO–SWS at a mean resolution of 1200 through emission in the ν_2 band at 14.98 μm (Lellouch *et al.* 1998, Feuchtgruber *et al.* 1999). Spectra were recorded at three positions with the $14'' \times 27''$ aperture aligned along the polar axis and successively centered on Jupiter's center, north pole and south pole, thus offering a moderate spatial resolution. These observations revealed a marked latitudinal variation, with the CO_2 emission being stronger in the southern hemisphere than at equatorial latitudes and undetectable in the northern hemisphere. No vertically-resolved information is available from these observations. Assuming that CO_2 is confined to levels above the ~0.5-mbar level (i.e., from comet SL9), Lellouch *et al.* (2002) derived column densities of $(6.3 \pm 1.5) \times 10^{14}$ in the south, $(3.4 \pm 0.7) \times 10^{14}$ in the equatorial region, and $<7 \times 10^{13}$ molecules cm^{-2} in the north. The CIRS spectrometer aboard *Cassini* also observed the CO_2 ν_2 band on Jupiter in December 2000 (Flasar *et al.* 2002) and confirmed this strong latitudinal variation.

7.2.6 Nitrogen, Sulfur, and Other Compounds

Ammonia, phosphine, hydrogen sulfide, water, germane, and arsine have been identified in Jupiter's troposphere through remote sensing or with the *Galileo* Probe Mass Spectrometer (see Chapter 4). Some of these species (e.g., NH_3, H_2S, and H_2O) will form condensates in the troposphere and are not expected to pass into the stratosphere through the tropopause cold trap. Others of these are disequilibrium species (e.g., PH_3, GeH_4, AsH_3) that may survive to reach the stratosphere or may be lost through photochemical processes in the upper troposphere. Detection of another disequilibrium tropospheric and potentially stratospheric molecule, HCN, was originally reported from ~13.5-μm ground-based observations of Tokunaga *et al.* (1981). However, more recent observations and a critical reanalysis of the Tokunaga *et al.* data set by Bézard *et al.* (1995) shed doubt on the reported HCN detection. Many different oxygen, nitrogen, sulfur, and metal species were observed in the jovian stratosphere following the 1994 impacts of Shoemaker–Levy 9. These observations are reviewed by Lellouch (1996) and in Chapter 8.

7.2.7 Spatial and Temporal Variability

Few published studies concerning the spatial variability of Jupiter's stratospheric composition have been presented for regions not perturbed by auroral phenomena. Early work on *Voyager* IRIS spectra by Maguire *et al.* (1984) revealed that the C_2H_6 mole fraction increased by a factor of three and the C_2H_2 mole fraction decreased by a factor of three from low latitudes toward the north pole. Preliminary work by the *Cassini* CIRS experiment team (Nixon *et al.* 2001) corroborates the Maguire *et al.* (1984) analysis and provides evidence for similar gradients from low latitudes toward the south pole. Using ground-based heterodyne spectroscopy, Kostiuk *et al.* (1983) and Kostiuk *et al.* (1987) obtained ethane abundances at five latitude points along the central meridian of Jupiter in 1981–1983 (+60°, +40°, 0°, −40°, −70° latitude). They found an increase in C_2H_6 emission and abundance near the south polar region relative to equatorial and northern latitudes, although the polar points may have been skewed by auroral effects. Mole fractions in the southern polar regions were typically as high as $\sim 5 \times 10^{-6}$, as compared with the relatively constant but lower values in the equatorial regions (average $\sim 2.8 \times 10^{-6}$). From 1989 measurements, Livengood *et al.* (1993) obtained $(3.6 \pm 0.9) \times 10^{-6}$ mole fraction at mid-latitudes and $(3.8 \pm 1.4) \times 10^{-6}$ at high latitudes outside the auroral region.

The question of temporal variability of hydrocarbon abundances in non-auroral regions is still unresolved due to the difficulty in separating temperature effects from abundance effects in analyses of infrared observations. Many of the differences reported in Table 7.1 reflect differences in modeling assumptions, including the use of different assumed temperature profiles. The possibility of temporal changes in mole fractions of photochemically produced species like C_2H_6 and C_2H_2 needs to be examined more systematically and carefully. Note that long-term temporal changes in C_2H_6 abundances in non-auroral regions have not been found to be significant in one study: retrieved mole fractions from measurements in 1982–1983 (Kostiuk *et al.* 1987) and 1986 (Kostiuk *et al.* 1989) yielded nearly identical mole fractions of $(2.8 \pm 0.6) \times 10^{-6}$.

Temporal and spatial variability can be very great within the auroral regions, however. Precipitating magnetospheric electrons and ions deliver $\sim 10^{14}$ W power to drive the aurora – an amount that exceeds the global solar extreme ultraviolet input by an order of magnitude (Atreya 1986; see Chapter 28). Spatial variability in hydrocarbon infrared emissions as a function of position within the auroral regions can result from both altered stratospheric chemical composition and altered temperature (see Section 7.4.1); typically, it is difficult to distinguish between the two possibilities for most observed species. Spectroscopy of auroral ultraviolet emission (e.g., most recently, Dols *et al.* 2000, Morrissey *et al.* 1997) reveals the signature of CH_4 and other hydrocarbons from extinction due to gas lying above the principal auroral source region. Dols *et al.* (2000) find fractional abundances for C_2H_6 and C_2H_2 relative to CH_4 that vary unpredictably with respect to auroral location or brightness (e.g., C_2H_2/CH_4 columns of 0.02–0.2 and C_2H_6/CH_4 columns of 0–0.5). As discussed in Section 7.2.4, Kim *et al.* (1985) identified substantial emissions by CH_4, C_2H_2, C_2H_4, C_2H_6, C_3H_4, and C_6H_6 in *Voyager* IRIS spectra of the auroral regions; some of these emissions were either not detected or only weakly detected elsewhere on Jupiter. Kostiuk *et al.* (1987) published a time-series of C_2H_6 spectra obtained at 60°N latitude during April 1982 that demonstrated a dip in emission intensity at the nominal auroral "hot spot" longitude, as compared with a three-fold enhancement seen in

a 1986 time series (Kostiuk *et al.* 1989). Livengood *et al.* (1993) have published an analysis of 1989 line-resolved C_2H_6 spectra in the northern auroral hot spot. The measured lineshape required a temperature increase as well as an increased C_2H_6 mole fraction of $(6.3–6.8) \times 10^{-6}$ compared to a non-hot-spot value at the same latitude ($\sim$60° N) of $(3.8 \pm 1.4) \times 10^{-6}$.

Ground-based infrared observations of C_2H_2 from Drossart *et al.* (1986) and C_2H_4 from Kostiuk *et al.* (1993) also demonstrated enhanced emission in the auroral regions. Kostiuk *et al.* (1993) found that the polar observation could be accounted for either by an increase in the nominal equatorial ethylene abundance or by a 67–137 K temperature increase in the 2- to 34-μbar pressure region compared to equatorial values, a temperature increase not inconsistent with the temperatures from H_2 quadrupole and H_3^+ emission lines in the auroral zones (see Section 7.4). Although it is difficult to to distinguish between mole fraction and temperature variations in explaining the polar emission enhancement, Kostiuk *et al.*'s arguments suggest that the C_2H_4 emission band observed by Kim *et al.* (1985) may be due to enhanced temperatures rather than greatly enhanced C_2H_4 column abundances.

7.3 CHEMICAL MODELS

Theoretical models have been developed to explain the observed composition of Jupiter's atmosphere. Thermochemical equilibrium, atmospheric transport, condensation, and photochemistry control the atmospheric composition in Jupiter's troposphere and stratosphere. Although some photolysis products of ammonia and phosphine may make it into Jupiter's stratosphere from their tropospheric production regions, methane is the most abundant equilibrium non-hydrogen-and-helium constituent that is volatile enough and stable enough to be transported throughout the stratosphere, where it can be affected by short-wavelength ultraviolet radiation. Methane photochemistry then acts to modify the composition of the jovian stratosphere. In this section, we discuss our current knowledge of stratospheric hydrocarbon and oxygen photochemistry on Jupiter; NH_3, PH_3, and H_2S photochemistry pertains mainly to the troposphere and is discussed in reviews by Strobel (1983), Atreya (1986), West *et al.* (1986), and Yung and DeMore (1999). The photochemistry of the vapor-phase molecules introduced to the jovian stratosphere following the Shoemaker–Levy 9 impacts is discussed in Chapter 8 (see also Moses *et al.* 1995a,b, Moses 1996, Lellouch *et al.* 2002).

7.3.1 One-Dimensional Photochemical–Diffusive Models

The distribution of atmospheric constituents in Jupiter's stratosphere can be predicted by considering the production, loss, and transport of each possible species at all locations in the atmosphere, as is described by the continuity equations (e.g., Gladstone *et al.* 1996). Eddy and molecular diffusion are typically considered in the transport terms. Throughout most of the stratosphere, large- and small-scale motions keep the atmosphere well mixed, and the eddy diffusion coefficient K provides a means for parameterizing this mixing. When the mean free path of atmospheric molecules becomes large in the upper stratosphere, molecular diffusion begins to take over from eddy diffusion. Near the homopause, which is the level where the eddy and molecular diffusion coefficients are equal, the atmospheric composition varies dramatically as the concentration of each constituent begins to be diffusively controlled and follows its own scale height. Most atmospheric constituents on Jupiter are heavier than the dominant gas, H_2; therefore, their scale heights are smaller than that of the bulk atmosphere, and their concentrations drop off sharply with altitude above the homopause. Because molecular diffusion coefficients differ for different species, each constituent has its own homopause level.

Molecular diffusion coefficients can be estimated using laboratory data (e.g., Marrero and Mason 1972) and standard gas-kinetic theory. Eddy diffusion coefficients cannot in general be rigorously derived from physical principles (cf. West *et al.* 1986), and the K profile is considered one of the main free parameters of jovian photochemical modeling. Numerous observations suggest that Jupiter has a stagnant lower stratosphere and upper troposphere (i.e., a low value of K in these regions). From *Voyager* IRIS observations of the ortho and para H_2 ratios, Conrath and Gierasch (1984) conclude that $K \lesssim 3000$ cm^2 s^{-1} near the 300 mbar level in Jupiter's upper troposphere. Observations of altitude variations of NH_3 and PH_3 (e.g., Lara *et al.* 1998, Edgington *et al.* 1998, 1999, Allen *et al.* 2001) and CH_3D (Parkinson *et al.* 2001) can also help constrain K in the upper troposphere. From thermal infrared observations of NH_3, Lara *et al.* (1998) determine that the eddy diffusion coefficient at 240 mbar varies from $\lesssim$400 to $\sim$4000 cm^2 s^{-1}, depending on latitude. Models of the NH_3 and PH_3 distributions based on ultraviolet HST–FOS observations (Edgington *et al.* 1998, 1999) also indicate a latitude dependence for K, and Edgington *et al.* (1999) find minimum values for K that fall in the range $\sim$200–600 cm^2 s^{-1} at 80–1000 mbar. Another way to determine $K_{\rm min}$, the minimum value of the eddy diffusion coefficient in Jupiter's atmosphere, is through measurements of the altitude distribution of tropospheric and stratospheric CO (Bézard *et al.* 2002). The results derived from CO observations are less sensitive to assumptions about photochemical stability than are determinations of $K_{\rm min}$ through NH_3 and PH_3 observations; however, the derivation of $K_{\rm min}$ from CO observations requires some knowledge of the influx rate of external oxygen to Jupiter. From an analysis of high-resolution observations of the CO band near 4.7 μm, Bézard *et al.* (2002) favor low values for $K_{\rm min}$ ($\sim$100–700 cm^2 s^{-1}) based on estimates of the CO influx rates due to impacts with Jupiter-family comets, but higher values of $K_{\rm min}$ cannot be ruled out.

Photochemical models are highly sensitive to $K_{\rm h}$, the eddy diffusion coefficient in the upper stratosphere near the methane homopause region (e.g., Atreya *et al.* 1984, Atreya 1986, Gladstone *et al.* 1996). Several different observations can be used to constrain $K_{\rm h}$. First, the observed fall-off of methane with altitude can provide a direct measure of the location of the methane homopause and hence the strength of atmospheric mixing. The altitude distribution of CH_4 in the homopause region has been inferred from *Voyager* UVS occultation results (Broadfoot *et al.* 1981, Festou *et al.* 1981, Atreya *et al.* 1981, Yelle *et al.* 1996), from ISO observations in the ν_3 band of methane near 3.3 μm (Drossart *et al.* 1999),

and from ground-based stellar occultation observations in the infrared (Drossart *et al.* 2000) (see Section 7.2.2). Unfortunately, the results do not always agree. As discussed in Section 7.2.2, very different results were derived by Festou *et al.* (1981) and Yelle *et al.* (1996) for the same UVS occultation data set because of the different assumptions adopted in the two analyses. The differences are not small – the inferred pressure level for the methane homopause differs by more than an order of magnitude between the Festou *et al.* and Yelle *et al.* analyses. From CH_4 observations, various groups have determined K_h to be (1–2) $\times 10^6$ cm^2 s^{-1} (Atreya *et al.* 1981), $1.4^{+0.8}_{-0.7} \times 10^6$ cm^2 s^{-1} (Festou *et al.* 1981), (0.1–2) $\times 10^7$ cm^2 s^{-1} (Yelle *et al.* 1996), (6–8) $\times 10^6$ cm^2 s^{-1} (Drossart *et al.* 1999), and $1.5^{+1.5}_{-0.8} \times 10^6$ cm^2 s^{-1} (Drossart *et al.* 2000).

Note, however, that when comparing different observational results, it is more useful to quote methane abundances at specific pressure or altitude levels than it is to quote eddy diffusion coefficients at the methane homopause. The latter result is highly sensitive to the assumed shape of the K profile, to the assumed temperature and density structure, and to assumptions regarding molecular diffusion coefficients – information that is often not provided in the published reports. Quotes of K_h that are several orders of magnitude apart can be consistent with each other if different assumptions have been adopted (e.g., Moses *et al.* 2000a). Conversely, similar derived values of K_h do not always indicate that the results regarding the inferred location of the methane homopause are consistent.

Eddy diffusion coefficients near the homopause region can also be derived from observations of the H Lyα airglow (e.g., Hunten 1969, Wallace and Hunten 1973, Broadfoot *et al.* 1981, Ben Jaffel *et al.* 1988, Skinner *et al.* 1988, Emerich *et al.* 1993) and from observations of the He I 584 Å airglow (McConnell *et al.* 1981, Vervack *et al.* 1995). Lyman-α emission from H in non-auroral regions results from resonant scattering of solar photons and interplanetary Lyα. Because methane strongly absorbs at Lyα, the emission derives mainly from H atoms residing above the methane homopause. The larger the eddy diffusion coefficient in the upper stratosphere, the higher the altitude to which the methane is mixed, and the smaller the column of atomic H that contributes to the emission, and hence the smaller the intensity of the Lyα emission. The 584 Å photons, on the other hand, are absorbed predominantly by H_2. Larger eddy diffusion coefficients in the helium homopause region lead to more helium being mixed into the upper atmosphere, and the resulting 584 Å emission intensity is increased. Note also that the results regarding He 584 Å emission refer to the helium homopause, not the methane homopause, and the two locations are not equivalent due to differences in molecular diffusion coefficients. Inferences about K_h from the above sources range from $\sim 1 \times 10^6$ to 3×10^8 cm^{-2} s^{-1}, with most values from the *Voyager* era and beyond lying in the (1–5) $\times 10^6$ cm^2 s^{-1} range. Determinations of K_h from He and H emission are complicated by the fact that emission intensities can be variable with time and with location on the planet (see Chapter 9 for more details). Values of K_h derived from methane observations may suffer from the same problem (e.g., Drossart *et al.* 2000). The effects of different assumptions regarding the eddy diffusion coefficient profile on stratospheric photochemistry are discussed in detail in Gladstone *et al.* (1996).

Once the diffusion coefficients and other transport terms are specified, the concentration of the different atmospheric constituents depends on chemical sources and sinks. The dominant photochemical pathways affecting the jovian stratospheric composition are discussed below (see also the reviews of Strobel 1983, Atreya 1986, Gladstone *et al.* 1996, Yung and DeMore 1999, Moses *et al.* 2000a; and Chapter 4).

7.3.2 Hydrocarbon Photochemistry

The problem of methane stability in Jupiter's upper atmosphere was first addressed by Wildt (1937), Cadle (1962), McNesby (1969), and Hunten (1969). The first to resolve the problem was Strobel (1969) (see also Strobel 1973, 1974, 1975), who recognized that long-lived disequilibrium products such as ethane and acetylene would be slowly transported down into the deep atmosphere, where they would encounter high temperatures and be converted back into methane. This "methane cycle" and associated hydrocarbon photochemistry is common to all the giant planets (see the reviews of Strobel 1983, Atreya 1986, Yung and DeMore 1999). The most recent comprehensive study of methane photochemistry in Jupiter's stratosphere has been presented by Gladstone *et al.* (1996) (see also Lee *et al.* 2000, Wong *et al.* 2000, Romani 1996, Allen *et al.* 1992, Landry *et al.* 1991, West *et al.* 1986, Yung and Strobel 1980, Atreya and Donahue 1979, Prasad *et al.* 1975). In the Gladstone *et al.* (1996) model, photochemical production and loss and vertical diffusive transport of hydrocarbons containing from one to four carbon atoms were calculated using a one-dimensional diurnally averaged model. Our knowledge of the hydrocarbon abundances (needed to test and/or constrain the models), kinetic reaction rate coefficients, ultraviolet absorption cross sections, and photolysis quantum yields (model input parameters) has improved tremendously since the Gladstone *et al.* (1996) model was developed. New models for jovian stratospheric photochemistry are needed. The discussion below is based largely on the updated photochemical models of Moses *et al.* (2000a) and Moses *et al.* (2001). The vertical profiles of the major hydrocarbon constituents in a recent model are shown in Fig. 7.2. The important photochemical pathways for producing and destroying the different hydrocarbons in this jovian stratospheric model are shown in Fig. 7.3. New models like the one shown in do an excellent job of fitting data for CH_4, C_2H_2, C_2H_6, and are within the upper limit for C_4H_2. The model shown also does a reasonable job at predicting the CH_3C_2H and C_6H_6 abundances but a poor job at predicting C_2H_4 abundances; the profiles for these last three species are particularly sensitive to poorly constrained model assumptions.

When CH_4 absorbs ultraviolet radiation, the molecule can be dissociated to form the short-lived radicals CH_3, CH_2, and CH. Methane absorbs ultraviolet photons with wavelengths less than ~145 nm. Because the solar Lyα line at 121.6 nm is the strongest UV source below 145 nm, direct methane photolysis on Jupiter is predominantly controlled by absorption of Lyα photons. The methane photolysis branching ratios at Lyα are poorly known. Recent laboratory experiments and theoretical calculations confirm that

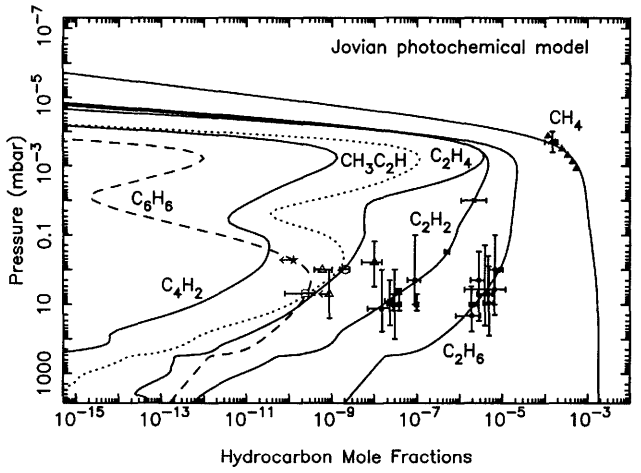

Figure 7.2. The mole fractions of the observable hydrocarbons in Jupiter's stratosphere as derived from a photochemical model developed for this chapter (based on Moses *et al.* 2001). The solid curves are the model profiles for individual hydrocarbons (as labeled), the dotted curve is for methylacetylene, and the dashed curve for benzene. The symbols with associated error bars represent data points. The solid triangles are for CH_4, the solid circles for C_2H_6, the solid squares for C_2H_2, the open triangles for C_2H_4, the open circle for CH_3C_2H, the star (upper limit) for C_4H_2, and the open square for C_6H_6. The K profile for this model is designed such that the CH_4 concentration is consistent with the results of Yelle *et al.* (1996).

the branch that forms methyl radicals (CH_3) is important (e.g., Mordaunt *et al.* 1993, Heck *et al.* 1996, Brownsword *et al.* 1997, Smith and Raulin 1999), as are branches that form methylene in the excited ($a\ ^1A_1$) state, $^1CH_2$ (e.g., Wang *et al.* 2000). Methyl radicals can react with atomic hydrogen to reform methane or with another CH_3 radical to form C_2H_6. Excited methylene radicals react with H_2 to form either CH_3 or $^3CH_2$ (ground-state $X\ ^3B_1$ methylene) and eventually CH. Insertion of CH into methane can produce C_2H_4; photolysis of C_2H_4 leads to the production of C_2H_2. Interchange between different types of C_2 hydrocarbons occurs through photolysis and through reactions such as H addition to C_2 molecules and radicals. These primary mechanisms for the production of C_2 hydrocarbons from direct methane photolysis have long been understood (e.g., Strobel 1975, Atreya 1986), but quantitative details are still evolving due to uncertainties in CH_4 photolysis branching ratios, in low-temperature absorption cross sections, and in low-temperature reaction rate coefficients. A recent review of hydrocarbon photochemistry (for Saturn) is presented by Moses *et al.* (2000a).

Methane photolysis occurs primarily just below the homopause region ($\sim 10^{-3}$ to 10^{-4} mbar), where CH_4 begins to become diffusively separated. Because of the large methane abundance on Jupiter, photons with wavelengths less than $\sim$145 nm are absorbed relatively high in the stratosphere, and methane photolysis is no longer effective at pressures greater than $\sim 10^{-2}$ mbar. However, photosensitized destruction of CH_4 still occurs in the middle and lower stratosphere through the photolysis of C_2H_2 and other hydrocarbons (e.g., Allen *et al.* 1980, Yung *et al.* 1984). Acetylene absorbs photons with wavelengths up to $\sim$230 nm. The ultimate dissociation products, C_2H and C_2, can react with H_2 to recycle C_2H_2 or with CH_4 to break apart the methane molecule. The former (recycling) process leads to the catalytic destruction of H_2 and to the production of H atoms. The latter process leads to the catalytic destruction of CH_4 and to the eventual production of C_2H_6 molecules and H atoms. The production of atomic H is of critical importance to the overall photochemistry in Jupiter's stratosphere, as sequential addition of H atoms can convert unsaturated hydrocarbons to saturated alkanes (e.g., C_2H_2 and C_2H_4 are converted to C_2H_6). The abundances of many of the observable hydrocarbons are very sensitive to the H-atom production rate.

Ethane is produced in Jupiter's stratosphere almost exclusively through three-body methyl–methyl recombination: $2\,CH_3 + M \rightarrow C_2H_6 + M$ (where M refers to any third body, such as H_2). Ethane production occurs throughout the stratosphere due to direct methane photolysis (upper stratosphere), photosensitized CH_4 destruction (middle and lower stratosphere), and C_2H_4 and C_2H_2 conversion (middle and lower stratosphere). Because of effective shielding by CH_4, loss processes like photolysis cannot keep up with ethane production, and like other alkanes, ethane is relatively unreactive and has a long chemical lifetime. Therefore, C_2H_6 is the most abundant of the disequilibrium hydrocarbons, and transport effects are important. Ethane builds up in the stagnant lower stratosphere and is removed largely by diffusion into the troposphere.

Ethylene is produced from $CH + CH_4 \rightarrow C_2H_4 + H$, from $C_2H_3 + H + M \rightarrow C_2H_4 + M$, and from photolysis of C_2H_6 and higher-order hydrocarbons. Loss of C_2H_4 occurs through photolysis (where C_2H_2 is the eventual product or the C_2H_4 is recycled) or through three-body addition reaction with atomic H (leading to the eventual production of C_2H_6 or CH_4). Ethylene is concentrated in the upper stratosphere because the main production mechanism (CH insertion into methane) occurs near the methane homopause, because there are no primary production schemes for C_2H_4 in the lower stratosphere, and because permanent loss processes involving the conversion of C_2H_4 to CH_4 and C_2H_6 become effective at lower-stratospheric pressures.

Acetylene is produced mainly from C_2H_4 photolysis, with a smaller contribution from C_2H_6 photolysis. Loss of C_2H_2 occurs through photolysis and H-atom addition. Recycling of C_2H_2 in the middle and lower stratosphere is much more prevalent than recycling of C_2H_4, and acetylene is therefore more abundant than ethylene in Jupiter's stratosphere. However, C_2H_2 recycling is apparently not as effective on Jupiter as it is on some of the other giant planets, as the C_2H_6/C_2H_2 ratio in the 0.1–1 mbar region on Jupiter (C_2H_6/C_2H_2 = 20–40) is larger than it is on Saturn (7–20) and Uranus (1–2), and is similar to that on Neptune (20–40). The reasons for these differences are not completely resolved (see Allen *et al.* (1992) for a more thorough discussion). Jupiter's warmer stratosphere may allow reactions that are highly temperature sensitive (e.g., $C_2H_3 + H_2 \rightarrow C_2H_4 + H$) to compete and help convert acetylene to ethane (Allen *et al.* 1992, Gladstone *et al.* 1996, Knyazev *et al.* 1996, Moses *et al.* 2001). Alternatively, Jupiter's smaller heliocentric distance and more energetic aurora may increase the production rate of atomic H, which can also provide a means for converting C_2H_2 to C_2H_6 (e.g., Fahr *et al.* 1995, Romani 1996, Moses *et al.* 2001). Other factors such as atmospheric transport may also play a role.

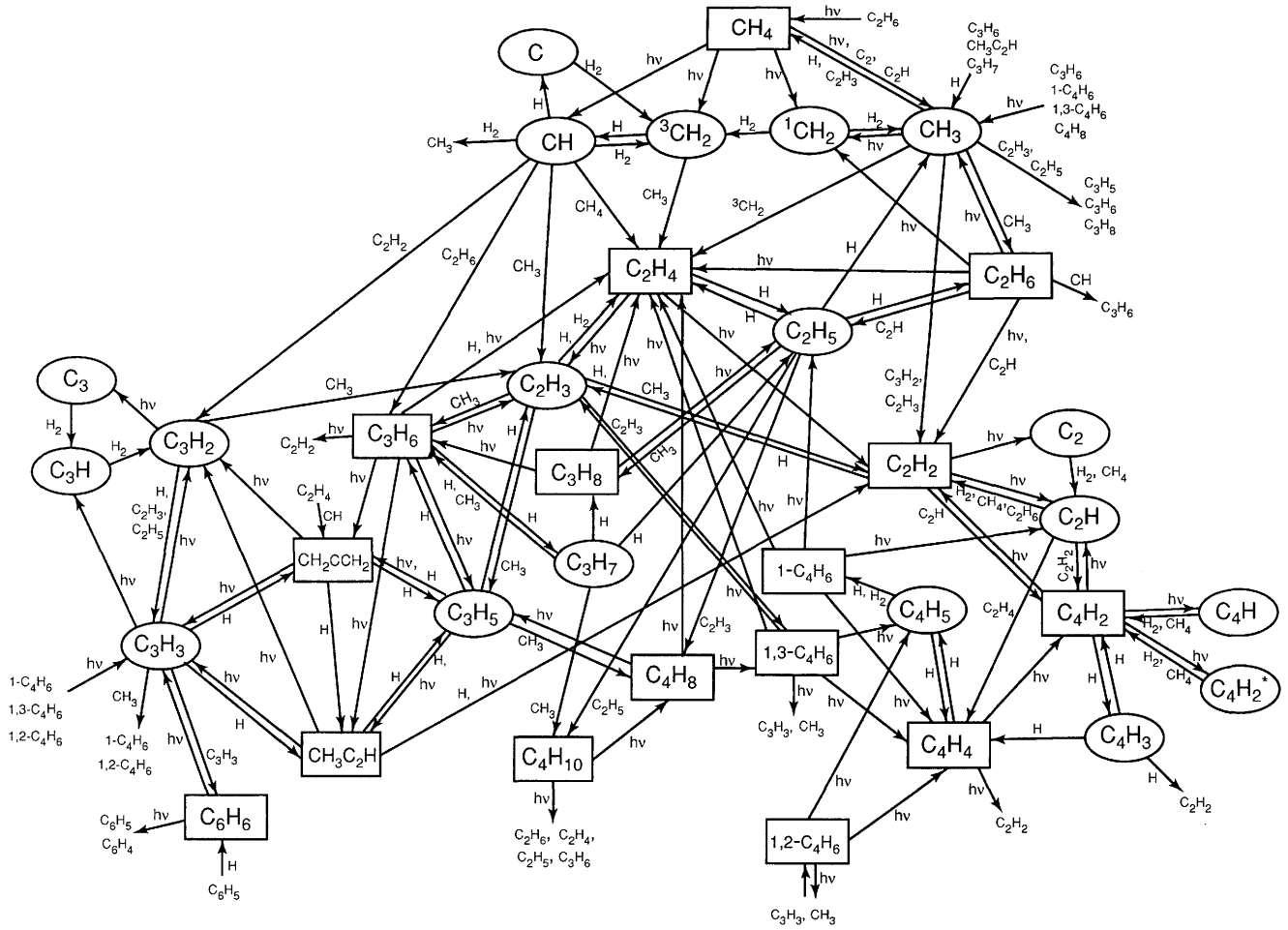

Figure 7.3. The important reaction pathways for producing complex hydrocarbons in Jupiter's stratosphere (after Moses *et al.* 2000a).

Due to a lack of relevant laboratory data, the photochemistry of C_3 hydrocarbons is less well known than that of C_2 hydrocarbons. The three mains mechanisms for producing C_3 hydrocarbons are CH insertion reactions (e.g., $CH + C_2H_6 \rightarrow C_3H_6 + H$), three-body radical-radical reactions (e.g., $CH_3 + C_2H_3 + M \rightarrow C_3H_6 + M$), and photolysis of C_4 and higher-order hydrocarbons. Important molecules like CH_3C_2H are probably produced from interconversion of other C_3 species rather than from direct production from C and C_2 hydrocarbons (Moses *et al.* 2000a). Again, the abundances of C_3 hydrocarbons seems to be highly sensitive to the H-atom production rate. In the model of Moses *et al.* (2001), methylacetylene is produced in the upper atmosphere through reactions ultimately driven by CH insertion into acetylene ($CH + C_2H_2 \rightarrow C_3H_2 + H$), followed by three-body addition reactions of C_3H_2 and C_3H_3 with atomic H. Photolysis of heavier C_3 and C_4 hydrocarbons helps produce CH_3C_2H in the middle and lower stratosphere. Methylacetylene is lost through photolysis and H-atom addition to form C_3H_5. However, both the photolysis products and C_3H_5 can recycle the CH_3C_2H, and methylacetylene survives much longer than its photolysis rate would indicate. Allene, another C_3H_4 isomer, is probably produced and destroyed in a similar manner, although conversion into CH_3C_2H may be an additional loss mechanism.

Other important C_3 hydrocarbons include propane (C_3H_8) and propylene (C_3H_6). In the Moses *et al.* (2001) model, the dominant mechanism for producing propane is $CH_3 + C_2H_5 + M \rightarrow C_3H_8 + M$, and propane is destroyed largely through photolysis. Like ethane, propane should be relatively stable in Jupiter's lower stratosphere. C_3H_6 is produced largely from CH insertion into C_2H_6 and from CH_3-C_2H_3 addition. Loss occurs through photolysis and reaction with atomic H. More laboratory data on low-temperature rate constants, reaction pathways, and absorption cross sections are needed before the details of C_3 hydrocarbon photochemistry can be worked out for Jupiter.

Diacetylene is the only C_4 hydrocarbon that has been detected on Jupiter, and its signature is found only in the auroral regions (see Section 7.2.4). This situation is different from that at Saturn, where emission from C_4H_2 is seen in disk-averaged spectra. C_4H_2 is likely produced in the middle and lower stratosphere at all latitudes through the photolysis of acetylene and the subsequent reaction $C_2H + C_2H_2 \rightarrow C_4H_2 + H$. Because the acetylene abundance is smaller on Jupiter than on Saturn, and because C_2H reacts preferentially with the more abundant H_2, CH_4, and C_2H_6 molecules, diacetylene production is not as efficient on Jupiter as it is on Saturn (cf. Moses *et al.* 2000a, 2001); and model predictions for middle and lower latitudes are

well within the upper limits provided by Fouchet *et al.* (2000). Other potentially important C_4 hydrocarbons include C_4H_{10}, C_4H_6, C_4H_8, and C_4H_4.

Benzene (C_6H_6) has been detected in both auroral and non-auroral regions on Jupiter (see Section 7.2.4). Its production mechanisms in low-temperature and pressure environments are uncertain both within the laboratory and within photochemical models. As discussed by Moses *et al.* (2000a), the formation of non-cyclic C_6H_6 molecules via C_3H_3–C_3H_3 recombination is likely to occur on the outer planets, and these molecules may be converted to the more thermodynamically favored form, benzene. Alternatively, reactions initiated by ion chemistry (e.g., Wong *et al.* 2000) might produce benzene in the auroral regions, and then the C_6H_6 molecules could be transported throughout the upper atmosphere. Note, however, that although the ion-chemistry mechanism proposed by Wong *et al.* (2000) may be sufficient to explain the high C_6H_6 abundances in the polar regions, the auroral-produced benzene will be diluted if spread globally; Bézard *et al.* (2001a) demonstrate that the auroral production as proposed by Wong *et al.* (2000) may fall short by as much as a factor of 50 in explaining the observed benzene abundance at low latitudes on Jupiter. Other proposed reactions such as $C_4H_5 + C_2H_2 \rightarrow C_6H_6 + H$ (e.g., Gladstone *et al.* 1996) or reaction of metastable excited acetylene $C_2H_2^*$ with two acetylene molecules (e.g., Strobel 1983) are not likely to be important due to high activation barriers or efficient collisional quenching of $C_2H_2^*$ with H_2. The high abundance of benzene on the outer planets is still a puzzle (see also Wilson and Atreya 2000).

7.3.3 Oxygen Photochemistry

The detection of H_2O, CO_2, and CO in the stratosphere of Jupiter (see Section 7.2.5) is intriguing because it implies that oxygen is entering the atmosphere from external sources (see Feuchtgruber *et al.* 1997, Moses *et al.* 2000b, Ollivier *et al.* 2000, Bézard *et al.* 2002, Lellouch *et al.* 2002). Possible sources include comets, interplanetary dust particles, and material from the planet's satellite and ring systems. Although the relative contributions from these different sources are still not well understood or well quantified, Lellouch *et al.* (2002) and Bézard *et al.* (2002) present mounting evidence that kilometer to sub-kilometer sized Jupiter-family comets (including Shoemaker–Levy 9) may be dominating the oxygen influx at Jupiter.

As discussed in Section 7.2.4, Lellouch *et al.* (2002) demonstrate that virtually all the H_2O and CO_2 recently observed in the stratosphere of Jupiter results from the 1994 impact of Shoemaker–Levy 9: (1) the water is confined to high altitude levels, higher than would be expected from a continuous meteoritic or ring/satellite source; (2) the CO_2 is most prevalent in the southern hemisphere (where the SL9 impacts occurred) and is not seen in the northern hemisphere; and (3) coupled photochemistry and transport models presented by Lellouch *et al.* (2002) show that the observed H_2O abundance and altitude distribution and the observed CO_2 abundance and horizontal distribution are consistent with the evolution of SL9-derived H_2O and CO at the impact sites (i.e., the CO_2 can be produced from the photochemistry of comet-derived H_2O and CO, and the H_2O is photochemically stable enough to last ~50 years after the impacts; see also Moses 1996). From the H_2O observations, Lellouch *et al.* (2002) place a strict upper limit of 8×10^4 cm^{-2} s^{-1} on the flux of H_2O from "continuous" meteoritic or ring/satellite sources. This conclusion differs from the situation on Saturn (e.g., Feuchtgruber *et al.* 1997, Moses *et al.* 2000b, Bergin *et al.* 2000), for which H_2O influx rates of $\sim 2 \times 10^6$ cm^{-2} s^{-1}, >25 times higher than on Jupiter, are inferred. Perhaps Saturn's water derives predominantly from a ring source, perhaps Saturn has experienced a recent cometary impact, or perhaps photochemistry or ablation chemistry result in different H_2O/CO partitionings at the two planets.

The CO observed on Jupiter, however, clearly does not all derive from the SL9 impacts. The fact that the CO mole fraction increases from the troposphere to the stratosphere implies a downward flux from an external high-altitude source, but Bézard *et al.* (2002) demonstrate that abundant CO exists at the *base* of the jovian stratosphere. Bézard *et al.* show that this CO cannot have been deposited during the SL9 plume splashback because the SL9-derived CO would take >300 years to diffuse from the splashback region (~0.1 mbar) to the tropopause bottleneck (~300 mbar), where it is observed today. To match the CO observations, Bézard *et al.* (2002) require stratospheric CO production rates of $(1.5\text{–}10) \times 10^6$ cm^{-2} s^{-1} for plausible minimum atmospheric eddy diffusion coefficients of 300–1500 cm^2 s^{-1}. Carbon monoxide is extremely stable in the jovian stratosphere and is the end product of much of the oxygen stratospheric photochemistry (see below). If oxygen enters the jovian atmosphere as oxygen ions (i.e., from the magnetosphere) that are quickly converted to O and OH, Strobel and Yung (1979) suggest that the O and OH could react with stratospheric CH_3 to form formaldehyde (H_2CO), and the H_2CO could then be photolyzed to eventually form CO. However, a magnetospheric source, with the oxygen originating from ring/satellite surfaces and Io's atmosphere, most likely cannot account for the observed CO because the globally averaged influx of oxygen is much too low (see the arguments given in Bézard *et al.* 2002).

Although influx of oxygen to Jupiter from interplanetary dust particles is estimated to be in the required range of $(1.5\text{–}10) \times 10^6$ cm^{-2} s^{-1} (see Moses *et al.* 2000b), the stringent upper limit of 8×10^4 cm^{-2} s^{-1} for the H_2O production rate (Lellouch *et al.* 2002) makes it seem unlikely that meteoritic material can account for the CO observed on Jupiter (e.g., Bézard *et al.* 2002, Lellouch *et al.* 2002). Ices within the dust grains will ablate at relatively low temperatures. Ice molecules can therefore ablate intact, although further collisions with atmospheric molecules might dissociate or ionize the ablated molecules. Because most of the ablation will occur above the methane homopause (see Moses *et al.* 2000b), the most likely fate of the ablated water would be to form O–H bonded ions and neutrals that will eventually reform water. We cannot imagine many situations in which CO production would dominate the ablation chemistry. One way might be for the dust grains to ablate completely below the methane homopause and for atomic O to be the dominant oxygen ablation product; in that situation, CO would become the main photochemical product and high CO/H_2O production ratios could be maintained, according to simulations based on the model of Moses *et al.* (2000b). Given the high entry velocities for meteoroids into

Jupiter's atmosphere (at least ~60 km s^{-1}), such a situation would require that most of the mass flux be deposited in very massive dust grains ($\gtrsim$10 g); otherwise, the micrometeoroids ablate at high altitudes. Alternatively, CO might form from the reaction of high-temperature silicate vapors with high-temperature organic vapors during the ablation of more refractory grain components. However, even if such reactions were plausible, the interplanetary dust grains encountering Jupiter would have to be relatively devoid of ices to maintain the high inferred CO/H_2O influx rate. The low upper limit for the "continuous" stratospheric production rate of H_2O therefore makes it unlikely that micrometeoroids contribute greatly to the external oxygen influx at Jupiter (Bézard *et al.* 2002, Lellouch *et al.* 2002), although that possibility cannot be completely ruled out given uncertainties in the chemistry of the ablated material.

The most plausible explanation may be that the CO observed on Jupiter derives from cometary impacts (Bézard *et al.* 2002). Carbon monoxide is generally the favored form of oxygen produced from shock thermochemistry in large cometary impacts at Jupiter (Zahnle 1996) and was certainly the dominant form of oxygen observed in the jovian stratosphere following the SL9 impacts (e.g., Lellouch 1996). Using estimated impact rates for Jupiter-family comets (Levison *et al.* 2000, Bottke *et al.* 1986), which are believed to be the most important group of jovian impactors, Bézard *et al.* (2002) estimate that sub-kilometer- to kilometer-sized comets could maintain a globally averaged CO production rate on Jupiter of $(0.2\text{–}1.7) \times 10^6$ cm^{-2} s^{-1}, with the range depending on uncertainties in the minimum atmospheric eddy diffusion coefficient K_{min} and on uncertainties in the cometary influx rate. The upper end of this range (corresponding to low values of K_{min}) is consistent with the production rate inferred from the CO observations.

High-spatial-resolution observations that allow the three-dimensional distribution of stratospheric CO_2 and H_2O to be derived for Jupiter and Saturn, and high-spectral-resolution observations that allow the altitude distribution of CO to be derived for Saturn, would shed light on the origin of external oxygen on these two planets. More realistic theoretical models (and/or laboratory experiments) regarding the fate of material introduced by the different possible sources would also be useful.

Regardless of whether the external oxygen is introduced by large cometary impacts or by more continuous micrometeoroid bombardment, the photochemistry of stratospheric oxygen compounds is expected to be similar – CO, H_2O, and CO_2 are expected to be the major endproducts (e.g., Prather *et al.* 1978, Moses *et al.* 1995a, Moses 1996, Moses *et al.* 2000b, Lellouch *et al.* 2002). Water can be dissociated at wavelengths less than 185 nm. However, shielding by CH_4, C_2H_2, and other hydrocarbons in the jovian stratosphere and recycling of the photolysis products back into H_2O allow water to persist for long timescales (e.g., Moses 1996, Moses *et al.* 2000b, Lellouch *et al.* 2002). Some of the water will be converted to CO following chemical schemes first suggested by Prather *et al.* (1978). Water photolysis leads to the production of OH, and the OH radicals can react with unsaturated hydrocarbons like acetylene and ethylene to eventually produce CO though a complex series of reactions (see Prather *et al.* 1978 and Moses *et al.* 2000b). The water that survives will diffuse into the lower stratosphere, where it can condense. Carbon monoxide is very stable in the jovian stratosphere. Both H_2 and CH_4 shield the CO and inhibit photolysis. Chemical loss processes are also inefficient. The slow reaction of CO with OH, leading to the production of CO_2, is the main loss process for CO and the main production mechanism for CO_2. Photolysis of CO_2 recycles the CO. Minor amounts of CH_3OH, H_2CO, and CH_3CHO can also form from the stratospheric oxygen photochemistry (e.g., Moses *et al.* 2000b).

In large cometary impacts, the comet-derived material will be relatively concentrated in the plume splashback regions in the months following the impacts, and oxygen compounds may interact with sulfur- and perhaps nitrogen-bearing constituents to produce transient photochemical species such as OCS, SO_2, and SO (Moses *et al.* 1995a,b, Moses 1996). These disequilibrium oxygen-bearing species are less likely to form with the more continuous meteoroid ablation scenario because of the greater likelihood of the ablated species encountering (and reacting with) jovian hydrogen and hydrocarbons. For more details on Shoemaker–Levy 9 impact observations and chemistry, see Chapter 8.

7.3.4 Modeling of the Auroral Regions

Although it has long been suggested that Jupiter's aurorae provide an important source of disequilibrium chemistry that may affect stratospheric composition on a global as well as local basis, most models to date have focused on low-latitude neutral photochemistry (e.g., Gladstone *et al.* 1996) or ionospheric chemistry (e.g., Kim and Fox 1994). Auroral chemistry has been relatively ignored. Simulations of the ion–neutral chemistry of the jovian auroral regions have been presented by Waite *et al.* (1983), Perry *et al.* (1999), and Wong *et al.* (2000). While the major chemical effect of precipitating auroral particles is the production of large amounts of atomic hydrogen (enough to dominate the global production of H by photochemistry), there is strong circumstantial evidence for an auroral chemistry pathway for producing Jupiter's ubiquitous auroral haze (e.g., West *et al.* 1986), a type of haze also present on Saturn (e.g., Ben Jaffel *et al.* 1995, Gérard *et al.* 1995) and probably the other giant planets as well (Pryor and Hord 1991). Aurora particles that penetrate the methane homopause initiate ion–neutral reactions that produce hydrocarbon ions such as CH_5^+, $C_2H_5^+$, $C_3H_5^+$, and c-$C_3H_3^+$; these ions are fairly unreactive and eventually recombine with electrons to provide a copious source of reactive radicals that can lead to the formation of more complex hydrocarbons.

Recently, Wong *et al.* (2000) used the auroral CH_5^+ recombination rates of Perry *et al.* (1999) to investigate a neutral path for polycyclic aromatic hydrocarbon (PAH) formation. As discussed in Chapter 5, these PAH molecules are known to be important precursors of soot particles, which are possible candidates for the auroral hazes. The implications of the Wong *et al.* (2000) results for aerosol formation have been investigated very recently by Friedson *et al.* (2002), who find quite good agreement with haze observations as far as the inferred size distribution and formation altitude are concerned; however, the predicted amount of aerosol loading in the Friedson *et al.* (2002) model is about two orders of magnitude lower than that required by observations (cf. Tomasko *et al.* 1986, West 1988, Rages, K. and

Beebe, R. and Senske, D. 1999), indicating that the production rate of condensible precursor gases is significantly underestimated by the chemical model of Wong *et al.* (2000). Wong *et al.* (2003) very recently updated these models to include ion-charge-exchange and electron-recombination reactions and, by analogy with Earth, more effective eddy mixing in the polar regions. Benzene and PAH production rates are significantly increased in the new model. Benzene attains a column abundance similar to the mid-latitude value derived by Bézard *et al.* (2001a), and the total volume of aerosol produced lies within the range allowed by the observations. However, much remains to be understood regarding chemistry and aerosol formation in the polar regions. More laboratory studies of the aromatic c-$C_3H_3^+$ ion, as well as other C_3 and C_4 ions would be helpful; c-$C_3H_3^+$ is more likely than CH_5^+ to be a terminal ion in Jupiter's auroral regions, as it is a product of several ion–neutral reactions and is apparently very unreactive (e.g., Anicich *et al.* 2000). The production of stratospheric haze in the auroral regions is discussed in more detail in Chapter 5.

7.3.5 Multidimensional Modeling

Although one-dimensional models are adequate for resolving the gross vertical structure of atmospheric constituents, horizontal transport effects may be important in determining the distribution of observable constituents in Jupiter's stratosphere. The intense auroral energy input in the polar regions affects stratospheric circulation (see Section 7.5 and Chapter 9), and Earth-based and spacecraft observations have become sufficiently detailed that latitudinal (and even longitudinal) differences in composition have become apparent (see Section 7.2). Two- and three-dimensional photochemical models are needed to resolve the finer details of horizontal, and even vertical, variations. Although no multidimensional models have appeared yet in the refereed literature, preliminary models have been discussed by Lee *et al.* (1998), Edgington *et al.* (2000), and Allen *et al.* (2000).

7.4 THERMAL STRUCTURE AND ENERGY BALANCE

7.4.1 Observations

Pre-*Voyager* observations relating to the thermal structure of Jupiter's stratosphere, including the results of the *Pioneer 10* and *11* missions, are reviewed by Orton and Ingersoll (1976); Kliore and Woiceshyn (1976); Hunten and Veverka (1976); Wallace (1976); Ridgway *et al.* (1976); Wallace and Smith (1976); Ingersoll (1976); and Gautier and Courtin (1979). Our focus in this chapter is on the major advancements since that time period.

The different observations pertaining to thermal structure can be classified as "density measurements" and "spectral measurements". For the density measurements, temperatures are derived from inferences about the atmospheric density structure as determined from refractive occultations

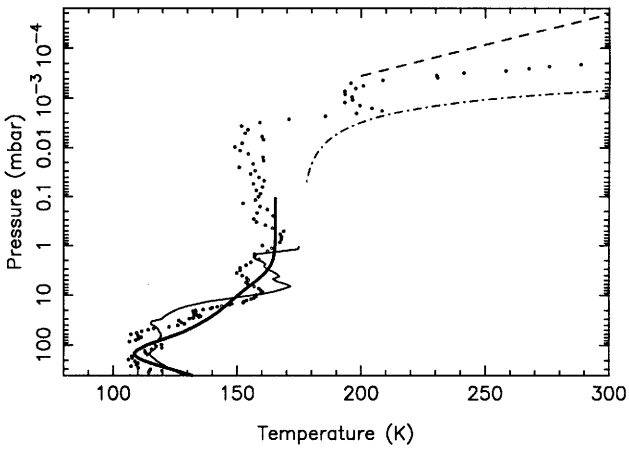

Figure 7.4. Temperature profiles determined for Jupiter's stratosphere. The thin solid line represents the *Voyager 1* egress radio occultation results from Lindal, 1992, as scaled by Conrath and Gautier, 2000. The dashed line represents the *Voyager* UVS occultation results as interpreted by Festou *et al.* (1981). The circles represent the *Galileo* probe ASI measurements (Seiff *et al.* 1998), and the thick solid line represents the analysis of various infrared data from ISO (Lellouch *et al.* 2001; see also Fouchet *et al.* 2000, Drossart *et al.* 1999). The dot-dashed line is Model C of Yelle *et al* 1996, which was derived from a reanalysis of the *Voyager* UVS occultation data set in combination with various other observations (see text).

(e.g., spacecraft radio occultations and visible stellar occultations), from absorptive occultations (e.g., ultraviolet stellar and solar occultations), and from velocity and deceleration data acquired when in situ probes traverse the atmosphere. The atmosphere is typically assumed to be in hydrostatic equilibrium and to behave as an ideal gas for deriving these temperatures, and some knowledge of atmospheric composition is necessary. For the spectral measurements, temperatures are derived from analyses of ultraviolet and infrared emission spectra. Each of these techniques has its strengths and weaknesses, and all are needed to piece together the stratospheric temperature profile on Jupiter.

Density Measurements

The gradual disappearance and return of radio signals as the *Voyager 1* and *2* spacecraft passed behind Jupiter were measured by receivers on the Earth. Analysis of the ingress ($-11.^\circ5$ to -13° latitude) and egress ($-0.^\circ6$ to $0.^\circ8$ latitude) radio occultation data for *Voyager 1* and egress (-57° to -73° latitude) for *Voyager 2* have been presented by Lindal *et al.* (1981). Results from the *Voyager 1* egress have been presented in tabular form by Lindal (1992), along with a thorough explanation of the assumptions made in the analysis. The radio occultations determine the vertical variation of the refractivity of the atmosphere; therefore, a composition must be assumed to determine pressure and temperature. Lindal (1992) adopted a He/H_2 ratio of 0.124, but more recent and direct *Galileo* results imply that the He/H_2 ratio is actually 0.157 ± 0.003 (von Zahn *et al.* 1998). Conrath and Gautier (2000) have rescaled the *Voyager 1* egress temperature profile to be consistent with the *Galileo* He abundance (see Fig. 7.4).

One way that the helium abundance was derived from the *Voyager* mission was through comparisons of the *Voyager* Radio Science Subsystem (RSS) temperature profile with IRIS thermal emission spectra (e.g., Gautier *et al.* 1981, Conrath *et al.* 1984). The possibility of systematic errors in the *Voyager* RSS results has been raised by Conrath and Gautier (2000) based on the disagreement between the *Voyager* and *Galileo* helium results. The rescaled RSS temperature profile appears to be inconsistent with the IRIS emission spectra – the new RSS profile is too warm by 2 K in the 200–500 mbar region. Unfortunately, investigations into the presence of systematic errors in the RSS analysis are difficult because Lindal *et al.* (1981) do not discuss the uncertainties in their results. Even if systematic errors were deemed to be present, it is not clear whether they would affect the tropospheric results only or the stratospheric results as well. A complete and separate reanalysis of the *Voyager* RSS occultation experiment is needed.

The rescaled RSS temperature profile shown in Fig. 7.4 has a temperature minimum of ~115 K at ~150 mbar. In the stratosphere, the temperature increases dramatically from a few tens of mbar to a few mbar and becomes more isothermal for pressures less than a few mbar. The RSS profile also exhibits a pronounced wave-like variation from 50 to ~1 mbar with a scale length of ~3 scale heights and an amplitude of ~10 K. Allison (1990) has interpreted the perturbation as the manifestation of equatorial Rossby waves. There are also smaller scale perturbations present, and Allison (1990) suggests that these may be inertia-gravity waves. Friedson (1999) and Leovy *et al.* (1991) identify the ~3-scale-height feature in the RSS profile as the the quasi-quadrennial oscillation (QQO) observed by Orton *et al.* (1991) in their maps of CH_4 7.8-μm emission. According to this explanation, the temperature variations oscillate with a period of 4 years (see discussion below).

The temperature profile in Jupiter's upper stratosphere and lower thermosphere has been studied through analysis of the *Voyager* UVS occultation experiment (Broadfoot *et al.* 1979, Atreya *et al.* 1979, Broadfoot *et al.* 1981, Festou *et al.* 1981, Yelle *et al.* 1996) and ground-based stellar occultations (e.g., Hubbard *et al.* 1995). These separate analyses find conflicting results. Hubbard *et al.* (1995) analyzed the occultation of SAO 78505 by Jupiter and derive a temperature of 176 ± 12 at 1.8 μbar. As shown in Fig. 7.4, Festou *et al.* (1981) derive a temperature profile that increases only gradually with height. Yelle *et al.* (1996) reanalyzed the UVS and ground-based stellar occultation data sets, utilizing information from solar-scattered emission in the H_2 Lyman and Werner bands (e.g., Liu and Dalgarno 1996b) and imposing the additional constraint that the temperature in the upper thermosphere be equal to the value of 800 K derived from analysis of H_3^+ emissions (e.g., Marten *et al.* 1994). Yelle *et al.* (1996) were able to find a temperature profile consistent with all four data sets. A primary characteristic of the Yelle *et al.* (1996) temperature profile is a large temperature gradient in the lower thermosphere (3–10 K km^{-1} at 0.3 μbar, in sharp contrast to the 0.55–0.65 K km^{-1} gradient determined by Festou *et al.* 1981). Subsequent direct measurements by the ASI experiment on the *Galileo* probe determined a temperature gradient for the mean profile of 3 K km^{-1} at 0.1 μbar.

The *Galileo* ASI instrument probed atmospheric temperatures from the thermosphere to well into the troposphere at Northern Equatorial Belt latitudes (6.5° latitude at probe entry). Of great benefit were the measurements in the middle stratosphere, a region that is hard to probe by any other methods. The ASI data have an altitude resolution that varies from 0.36 to 0.11 km. The derived temperatures are accurate to 0.12 K (Seiff *et al.* 1998). Systematic uncertainties in temperature related to starting conditions can be large in the upper thermosphere but are mostly absent at pressures greater than ~0.1 mbar, and the values quoted above should reflect the absolute accuracy of the derived temperature (Seiff *et al.* 1998). The basic features of the ASI profile are consistent with the RSS profile (see Fig. 7.4), though there are differences in detail. Both profiles possess a strong gradient that extends from 100 to ~10 mbar, at which point the atmosphere becomes roughly isothermal, except for quasi-periodic smaller scale variations.

The good altitude resolution and precision of the ASI measurements reveal numerous small scale variations in the temperature profile that are probably due to waves in the atmosphere (Seiff *et al.* 1998). The deviations of the actual temperatures from the mean profile are well outside the accuracy of the ASI measurements, so there is little doubt about the reality of the perturbations. The ASI measurements reveal a much richer spectrum than is evident in the RSS profiles. Because it is impossible to produce these variations with radiative processes, they must be dynamical in origin. The wave-like perturbation between ~50 and 1 mbar, first seen in the RSS experiment, is also present in the ASI results. Friedson (1999) argues that this perturbation is consistent with the QQO oscillation. The smaller scale perturbations are likely manifestations of inertia-gravity waves. The region of static stability associated with the stratosphere extends over ~5 decades of pressure. Thus, gravity waves will travel a large distance in the stratosphere, and small temperature perturbations in the troposphere will create easily detectable waves in the upper stratosphere. Assuming that the waves grow as the inverse square root of density, a wave amplitude of 0.1 K at the tropopause will grow to 10 K by 0.01 mbar. It would be hard to avoid large-amplitude gravity waves in the upper stratosphere.

The onset of the large temperature gradient at pressures of a few tenths of a microbar to a microbar suggests an intimate connection to the disappearance of hydrocarbons (e.g., Yelle *et al.* 1996), whose abundances decline rapidly in this region due to diffusive separation. The coincidence of the large temperature gradient and the homopause suggests that the temperature increases because of the absence of cooling supplied by hydrocarbons. The main constituents of Jupiter's atmosphere, H_2 and He, are inactive and radiate away no energy at the pressures under consideration here. Thus, hydrocarbons, though sluggish radiators themselves, provide the only avenue for radiative cooling. In addition, the breakdown of local thermodynamic equilibrium at high altitudes may be contributing to the temperature increase at the top of the stratosphere, as cooling through the ro-vibrational bands of the hydrocarbons becomes less effective in this situation.

Spectral Measurements

Temperatures can be derived from ultraviolet emission spectra that have sufficiently high spectral resolution. From an analysis of emission in the H_2 Lyman and Werner bands, Liu and Dalgarno (1996b) derived a temperature of 500–600 K at $\sim 3 \times 10^{-4}$ mbar, near the methane homopause region; they were the first to demonstrate that high temperatures could exist at relatively high pressures in Jupiter's upper atmosphere. Their results are in serious conflict with the shallow temperature gradient advocated by Festou *et al.* (1981) (see above).

Infrared observations have been more fruitful than ultraviolet observations in inferring temperatures in the middle and lower stratosphere of Jupiter. Observations of emission in the ν_4 band of CH_4 (7–8 μm) by Gillett *et al.* (1969) were the first to indicate that Jupiter's stratosphere is unexpectedly warm. The fact that optical depth unity is reached in the stratosphere at the center of the CH_4 ν_4 band implies that Jupiter's stratosphere is "inverted," i.e., that temperatures increase with altitude in Jupiter's stratosphere. This interpretation was corroborated by center-to-limb studies that show limb brightening (Gillett and Westphal 1973, Orton 1975b) and by 20-μm center-to-limb brightness observations from the *Pioneer 10* and *11* Infrared Radiometer (Orton 1975a) that indicate the existence of a nearly isothermal region near the 100-mbar pressure level. The stratospheric heating was suggested by Gillett *et al.* (1969) to be caused by absorption of sunlight in the 3-μm ν_3 band of CH_4. Detailed radiative models by Hogan *et al.* (1969), Cess and Khetan (1973) and Wallace *et al.* (1974) verified this numerically. More recent radiative equilibrium models (e.g., Yelle *et al.* 2001) demonstrate the importance of all the near-infrared methane bands, including the bands at 1.1, 1.3, 1.7, 2.3, and 3.3 μm, in heating the stratosphere.

The first attempts to derive temperatures directly from the data were made by Ohring (1973) and Orton (1975b), with subsequent work providing improvements to the radiative transfer calculations (Orton and Aumann 1977). With the spectral resolution of the early data ($\Delta\nu \sim 20$ cm^{-1}), it was possible to retrieve only one point on the temperature profile, at a pressure level of 10 mbar. As noted by Wallace and Smith (1976), deriving a unique solution to the temperature profile in the lower stratosphere from a single data point is not possible. The fact that the Planck function at 8 μm is such a strong function of temperature for this cold thermal region means that the hotter pressure levels overlying the 10-mbar level also contribute to the outgoing radiance. Consequently, solutions to the temperature profile in this region require initial guesses that are "conditioned" by independent information, such as direct in situ observations or radio occultation results.

The next significant analysis of the jovian infrared spectrum to derive stratospheric temperatures was that of the *Voyager* IRIS team (e.g., Hanel *et al.* 1979b,a), who also used the strong ν_4 band of CH_4 at 7.7 μm. With a spectral resolution of $\Delta\nu \sim 4.3$ cm^{-1}, the IRIS instrument resolved the P, Q and R branches of the ν_4 band. This improvement, together with the knowledge of the upper troposphere temperatures derived from the *Voyager* occultation measurements, allowed the inversion of the stratospheric temperature profile between 30 and 3 mbar. In addition, Gautier *et al.* (1982) used the IRIS spectra to improve significantly the accuracy (±10%) of the CH_4 mole fraction measurement, an essential parameter for the reliability of the temperature inversion. The ISO–SWS spectrum of Jupiter (Encrenaz *et al.* 1996, Fouchet *et al.* 2000) and spatially resolved *Cassini* CIRS observations have improved the spectral resolution to below 1 cm^{-1}. However, as shown by Gautier and Revah (1975), retrieving the temperature profile on vertical scales smaller than the atmospheric scale height is difficult or impossible in practice; typically, no more than four independent points on the temperature profile can be determined between 30 and 1 mbar.

The non-uniqueness of the inverted profile remains a problem when *a priori* information on upper stratosphere temperatures is unavailable. In particular, the inverted profile is highly sensitive to the assumed temperature around a few tens of a μbar, where the CH_4 line Doppler cores reach an optical depth of 1. However, some of the problems may be alleviated with high-spectral-resolution observations that allow the resolution of strong and weak CH_4 lines. For example, using the Irshell spectrometer at a resolution of $\Delta\nu \sim 0.07$ cm^{-1}, Bézard *et al.* (1997) showed that the stratospheric heating due to the Shoemaker–Levy 9 impacts was confined to pressures less than 0.1 mbar. Measurements at even higher resolution, capable of resolving the line shape of individual lines, can provide significant constraints on the temperature as well as abundance.

More recently, the ISO–SWS instrument detected the $S(0)$ and $S(1)$ H_2 quadrupolar lines in the globally averaged jovian spectrum (Fouchet *et al.* 2000, Lellouch *et al.* 2001); these quadrupole lines had been detected before by Kim *et al.* (1990), but only in observations of the southern auroral region. These transitions are so weak that, despite the high H_2 abundance, they probe a broad pressure region centered on a few mbar. Hence, they provide an independent method to probe the temperature in the lower stratosphere. When coupled with the methane measurements, H_2 quadrupole line observations can provide an additional check on the results derived from the CH_4 observations and therefore can help resolve the non-uniqueness problem in the inversion of the stratospheric temperature profile. The stratospheric profile derived from ISO–SWS observations (averaged over middle and lower latitudes) is shown in Fig. 7.4. This profile is constrained by the H_2–He continuum in the 13–16 μm region and in microwindows in the 7–9 μm region (sensitive from the tropopause to 500 mbar), by CH_4 emission in the ν_4 band (sensitive to the ~1–35 mbar pressure region), and by the $S(0)$ and $S(1)$ quadrupole lines of H_2 (broad contribution functions that peak near 25 and 5 mbar, respectively) and is described in more detail in Lellouch *et al.* (2001) and references therein.

Temperatures in the Auroral Regions

A relatively constant feature of the north polar stratospheric temperature field is a "hot spot" area located at roughly 60° N, 180° W longitude in System III; the feature was discovered in IRTF scans of CH_4 infrared emission (Caldwell *et al.* 1980) and was recognized *a posteriori* in the *Voyager* IRIS data (e.g., Kim *et al.* 1985). The properties of this nominal hot-spot region have been documented further by Caldwell *et al.* (1983), Caldwell *et al.* (1988), and Halthore

et al. (1988). The location of the feature within the auroral oval is consistent with it resulting from localized heating of the neutral atmosphere by energetic particle bombardment (Prangé 1991, Livengood *et al.* 1990, Livengood and Moos 1990). More recently, the source of thermal emission has been determined to be co-located with the source of auroral-related X-ray emission (e.g., Gladstone *et al.* 2002). Within the hot-spot region, enhanced thermal emission from other hydrocarbons such as C_2H_2, C_2H_6, and C_2H_4 has also been observed from *Voyager* IRIS data (Kim *et al.* 1985) and from ground-based observations (e.g., Drossart *et al.* 1986, Livengood *et al.* 1993, Kostiuk *et al.* 1993). These ground-based observations probe different pressure regions and have provided information on the stratospheric thermal profile.

A similar south polar thermal emission feature near 70° S is more peripatetic – it wanders in longitude from 330° W through 60° W in System III – and is more ephemeral than its northern counterpart (Caldwell *et al.* 1983). The northern auroral hot spot also has had periods during which it was not observed: the feature was absent in many observations taken in the early 1990s, it appeared in 1994 prior to the SL9 impacts, it did not appear during the actual time frame of the SL9 impacts, and it has inconsistently appeared since that time. The timescale for its appearance and disappearance is shorter than ~1 month but seems to be longer than several days. Systematic quantitative studies of the time dependence of this phenomenon are needed, as are quantitative physical models.

The hot spots are not necessarily consistently "hot" in emissions of all stratospheric species. Kostiuk *et al.* (1987) typically found little or no enhancement in C_2H_6 emission at the hot spots in 1982–1983 observations and even observed a pronounced dip in C_2H_6 emission intensity in a northern auroral hot-spot region in April 1983. Livengood *et al.* (1993), in observations from 1989, found a C_2H_6 integrated line intensity that was enhanced by a factor of ~6 relative to quiescent emission on one day, a factor of ~2 on the following day, returning to a factor of ~6–7 enhancement four days later. Since the photochemical lifetime for C_2H_6 is extremely long ($\gtrsim$100 years), much longer than timescales for horizontal transport away from the hot-spot region, the variability in emission must be at least partly due to local heating in the stratosphere. The requirement of enhanced local temperatures on at least some occasions is confirmed by the brightest measurements in the 1989 data set of Livengood *et al.* (1993), in which line-center brightness temperatures significantly in excess of zonally averaged temperatures (e.g., Maguire *et al.* 1984) were obtained. Such temperatures are sufficient to account for much of the observed enhancement and variability in emission by C_2H_6, C_2H_4, and other hydrocarbon species in the auroral region.

Observational constraints on the auroral stratospheric thermal profile are limited at this point in time. From 3–4 μm spectroscopy of auroral H_3^+ emissions, temperatures of 700–1150 K have been derived for thermospheric pressures less than ~1 μbar (e.g., Maillard *et al.* 1990, Kim *et al.* 1993, Drossart *et al.* 1993b, Lam *et al.* 1997, Mai and Jockers 2000). An analysis of spectrally resolved C_2H_4 lines at 10.5 μm has yielded a temperature of ~250–320 K at 2–34 μbar (Kostiuk *et al.* 1993) from a 1989 observation. A recent re-evaluation of the jovian equatorial C_2H_4 column density (Bézard *et al.* 2002) may lower the estimated quiescent abundance and thus require even greater temperatures to explain these auroral spectra. Spectroscopy of C_2H_6 lines at 11.8 μm has allowed both the local C_2H_6 abundance and the temperature to be constrained for the time of the observations; the results imply an enhanced C_2H_6 mole fraction (6.6×10^{-6} as compared with 3.8×10^{-6}) and an enhanced temperature of 183 K (10–12 K warmer than the non-auroral atmosphere) in the 0.3–3 mbar region (Livengood *et al.* 1993). These C_2H_4 and C_2H_6 measurements were contemporary but not simultaneous. Drossart *et al.* (1993a) investigated thermal profiles in an attempt to match *Voyager* IRIS spectra of thermal emission in the auroral region. They found a family of thermal profiles with temperatures at ~10–20 μbar that were enhanced to 300–400 K – a range that is consistent with the C_2H_4 results of Kostiuk *et al.* (1993). Spectroscopy of ultraviolet auroral H_2 emissions also has been analyzed for temperature information preserved in the rotational distribution of impact-excited H_2; the results have yielded temperatures of 400–600 K (Trafton *et al.* 1994, Liu and Dalgarno 1996a, Kim *et al.* 1997, Dols *et al.* 2000) at an inferred pressure region of a few microbars; i.e., between the regions probed by the hydrocarbon emissions (2–34 μbar) and the H_3^+ emissions ($\lesssim$1 μbar). Quadrupole emissions of H_2 at 2 μm yield temperatures of 530–1220 K for the 0.1–1 μbar pressure region of the lower thermosphere (Kim *et al.* 1990), values that are consistent with the H_3^+ thermospheric temperature and with an implied source for the UV auroral emission at a few microbar.

A recent stellar occultation event on October 10, 1999, promises to provide powerful independent constraints on the thermal profile in the auroral region (e.g., Raynaud *et al.* 2003). Spectroscopy of H_3^+ emission was acquired simultaneously with the occultation, providing a direct comparison between methods, but unfortunately, spectroscopy of stratospheric hydrocarbons was not obtained at that time. The variability of the auroral energy input suggests that temperatures within the auroral region will be significantly variable and require simultaneous observations with multiple techniques to understand the physics of the region. The auroral thermal profile thus awaits concerted investigation.

Non-Auroral Spatial and Temporal Variability

The spatial and temporal variability of Jupiter's stratospheric thermal structure has been documented observationally since 1979, starting with the *Voyager* IRIS experiment and continuing with ground-based infrared observations of filtered radiance in the 7.8-μm CH_4 emission feature. Early ground-based observations consisted of spatial scans of the central meridian (e.g., Sinton *et al.* 1980, Beebe *et al.* 1989), whereas observations taken after 1984 (see Orton *et al.* 1991) took advantage of efficient two-dimensional raster scanning from the NASA Infrared Telescope Facility (IRTF). Deming *et al.* (1989) employed a one-dimensional detector array to observe in broadband flux over 8–13 μm; they discovered low-wavenumber non-acoustic thermal wave structure in Jupiter's upper troposphere and lower stratosphere. This phenomenon was investigated further by Deming *et al* (1997). Two-dimensional imaging arrays sensitive to mid-infrared wavelengths first came into use in 1993 and were used to monitor the atmospheric perturbations associated with the impact of Shoemaker–Levy 9 with Jupiter

(Orton *et al.* 1995, Livengood *et al.* 1995, Lagage *et al.* 1995, Billebaud *et al.* 1995). Two-dimensional imaging arrays were also used to characterize the *Galileo* probe entry site (Orton *et al.* 1998). Since the 1995 epoch, mid-infrared imaging observations have accompanied nearly every planned *Galileo* atmospheric observing sequence (e.g., Orton *et al.* 2001).

All spatial variations in Jupiter's stratospheric temperature field are time dependent. The simplest spatial variability is the northern and southern hemispherical asymmetry that is a slow function of time; this asymmetry is evident in the time series of meridional variations of Jupiter's stratospheric temperatures shown in Fig. 7.5. Despite Jupiter's small (3°) obliquity, seasonal variations of insolation are believed to be responsible for the asymmetry (e.g., Beebe *et al.* 1989). The amplitude and phase of the variations correspond roughly to those in the time-dependent radiative-convective model of Bezanger *et al.* (1986), but no detailed study has yet been made of the dependence of the results on various assumptions about radiative heating mechanisms, such as the effectiveness of particulate *vs.* gaseous absorption or the possible seasonal time dependence of the abundances of the radiatively cooling gases like C_2H_2 and C_2H_6.

Superimposed on the seasonal variations is a time-dependent meridional organization that is also evident in Fig. 7.5. The positions of temperature maxima alternate in time between the equator and low to mid-latitudes (±15°). The placement of these bands has no ostensible relationship with the tropospheric temperature field, which is anticorrelated with the bright and dark bands of the visible cloud field. Nonetheless, the latitudes of the warm mid-latitude bands are similar to those of the warm stratospheric bands in the radiative–convective–dynamical model of Conrath *et al.* (1990). The alternating maxima at mid-latitudes and equator as a function of time were noticed by Orton *et al.* (1991), with Leovy *et al.* (1991) suggesting that the phenomenon was a quasi-periodic oscillation of the zonal wind and longitudinally averaged temperature, similar to the Earth's quasibiennial oscillation (QBO). They named the phenomenon the quasi-quadrennial oscillation, or QQO, for its roughly 4-year period. Numerical models of these results were generated by Friedson (1999), who determined that the amplitude of the QQO could greatly exceed the apparent amplitude seen in the brightness temperature variations, which are smoothed by the large vertical extent of the 7.8-μm weighting function. As a result, he concluded that the interaction of small-scale, short-period gravity waves with the zonal mean flow is likely to be driving the QQO. This interpretation implies the existence of a large-scale vertical temperature oscillation associated with the QQO; such an oscillation was in fact observed by the *Galileo* probe ASI experiment (see above). Further modeling by Li and Read (2000) confirms that the QQO may result from interactions of a small number of equatorially trapped wave modes with the stratospheric zonal flow.

Besides the slow quasi-periodic oscillations, the thermal images at 7.8 μm show ample evidence for horizontal (largely zonal) waves in the temperature field. These thermal waves are qualitatively similar to their counterparts in the troposphere (e.g., Magalhães *et al.* 1989, 1990). The most prominent stratospheric wave amplitudes lie between 30° N and 20° S latitudes. The wavenumbers with the greatest amplitude in a power spectrum lie between 3 and 11.

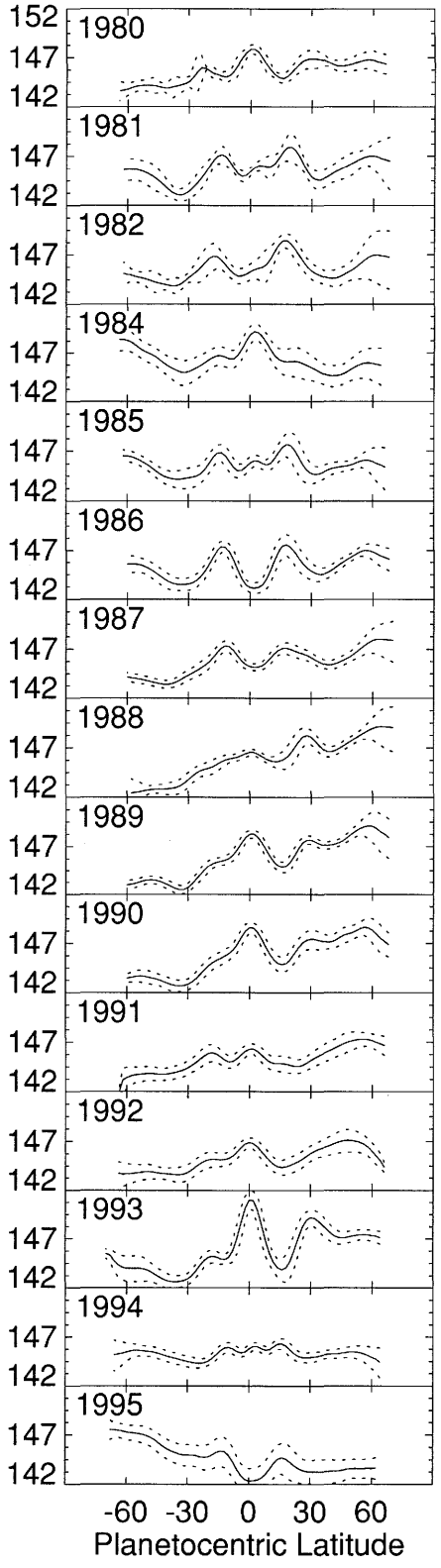

Figure 7.5. Meridional profiles of jovian zonal mean 7.8-μm brightness temperatures (K) for the years 1980–1995, corrected for emission angle and Doppler effects (adapted from Friedson, 1999). Data for the year 1983 were extremely noisy and hence are not included. Dashed lines represent ±1 standard deviation of brightness temperatures about their zonal average.

The phase speed of these waves appears to be slow with respect to System III, on the order of ~20 m s^{-1} retrograde, but variations up to 10 m s^{-1} from this value exist for different waves at different times. Wave trains are occasionally seen to follow prominent thermal features that are up to 2 K higher than their surroundings and as wide as 15 000 km. The fact that these waves are strongest at ±20° latitude may be related to the prominence of large-scale zonal variations of temperature in the upper troposphere. Conrath *et al.* (1981) suggest that these tropospheric thermal fluctuations are related to the retrograde jets at ±18° planetocentric latitude in Jupiter's troposphere; the waves are expected to be highly susceptible to instability associated with the horizontal zonal wind shear. Orton *et al.* (1991), in turn, suggest that it is possible that the stratospheric waves originate as instabilities in the troposphere and propagate upward, increasing their amplitude as the background atmospheric density decreases with altitude. They cite one instance in which the zonal variation of tropospheric (~250-mbar) temperatures is recognizable in the zonal variation of stratospheric temperatures some 4 months later. This upwelling wave phenomenon has not been verified systematically.

When temperature perturbations affect the structure of the jovian stratosphere, the atmosphere will decay back to the radiative equilibrium state over a certain timescale, the radiative relaxation time (τ_{rad}). Taking into account only the H_2–He pressure-induced absorption, Flasar (1989) calculated that τ_{rad} in Jupiter's stratosphere varies from ~500 days at the tropopause to ~1000 days at the 10-mbar level. Bézard (1997) added molecular band opacity from the main hydrocarbons CH_4, C_2H_6, and C_2H_2 and found that τ_{rad} decreases from ~1000 days at the 10-mbar region to a minimum of 10–20 days at pressure levels of a few microbars. This decrease results from the increasing emissivity of the atmosphere due to larger relative hydrocarbon abundances and lower atmospheric opacity. The radiative relaxation time then reaches a minimum just below the homopause region where the C_2H_6 and C_2H_2 mole fractions are highest. Above the homopause, the τ_{rad} is expected to increase rapidly due to the decline of the hydrocarbon profiles and to the breakdown of local thermodynamic equilibrium at high altitudes. Note that these calculations strongly depend on the assumed vertical profiles of CH_4, C_2H_6, and C_2H_2.

7.4.2 Radiative Equilibrium Models

Cess and Khetan (1973) and Wallace *et al.* (1974) conducted the first successful radiative equilibrium calculations of the thermal profile in the jovian stratosphere. Wallace *et al.* correctly identified the near-infrared CH_4 bands as the main source of heating in the stratosphere, and models including these bands alone and cooling through the ν_4 band of CH_4 matched the measurements of the stratospheric temperature available at the time. Wallace *et al.* did not include radiative cooling by C_2H_2 and C_2H_6 in their calculations but estimated that significant amounts of these molecules could cool the upper stratosphere by tens of kelvins. Cess and Chen (1975) improved their models by including cooling by C_2H_2 and C_2H_6. Using constant abundances of $C_2H_6/H_2 = 1 \times 10^{-5}$ and $C_2H_2/H_2 = 5 \times 10^{-7}$, Cess and Chen found that ethane and acetylene cooled the stratosphere by 20 K. The models were then cooler than temperatures inferred from observations. In order to bring the models back into agreement with the observations, Cess and Chen hypothesized the presence of significant aerosol heating. Appleby and Hogan (1984) and Appleby (1990) continued studies of Jupiter's thermal structure, motivated partly by the availability of *Voyager* measurements. They included aerosol heating in a parameterized fashion and found that the aerosols must absorb 3.8% of the total solar flux in order to bring the models into agreement with temperatures inferred from the *Voyager* radio occultation experiment. Acetylene and ethane were included in these models using the same formalism and same mixing ratios as Cess and Chen (1975). The relative importance of cooling by CH_4, C_2H_2, and C_2H_6 was not discussed.

Later models considered the two-dimensional structure (latitude and altitude) of the stratospheric temperature field and included the effects of dynamics (e.g., Conrath *et al.* 1990, West *et al.* 1992, Moreno and Sedano 1997). In the model of Conrath *et al.* (1990), realistic seasonal radiative forcing was included, but aerosol heating was omitted. Horizontal temperature gradients in the stratosphere were found to be very small (i.e., temperatures at any particular middle or lower stratospheric pressure were constant to within $\lesssim$3 K), except within ~20° of the poles. West *et al.* (1992) and Moreno and Sedano (1997) expanded the models to include the effects of aerosol heating; they emphasized the consequences with regard to stratospheric dynamics, and their results are discussed more fully in the next section.

Yelle *et al.* (2001) re-examined radiative processes in the jovian stratosphere, relying upon constraints provided by the ASI temperature profile and various recent measurements of the stratospheric composition. Cooling rates from hydrocarbons were calculated based on realistic altitude profiles of CH_4, C_2H_2, and C_2H_6 that are roughly consistent with predictions from photochemical models. Heating and cooling rates in the stratosphere are shown in Fig. 7.6. One interesting result from the Yelle *et al.* model is that, contrary to many earlier studies, heating by aerosols is found to be of negligible importance in the equatorial regions. In addition, the primary coolant through much of the stratosphere is C_2H_6. This result reveals a much stronger link between stratospheric photochemistry and energetics than had previously been appreciated (see Section 7.5 below).

Departure of the three-dimensional thermal structure from its radiative equilibrium state provides information about the role of dynamics in the stratosphere. *Voyager* and ground-based observations indicate that the stratospheric temperature is surprisingly uniform with latitude, implying efficient meridional redistribution of heat. The implications of these observations for the stratospheric circulation and the transport of trace constituents are discussed in Section 7.5.

7.5 MERIDIONAL TRANSPORT

Compared to Earth, we know very little about transport in Jupiter's stratosphere. The primary impediment is the paucity of data concerning winds at altitudes above the uppermost tropospheric cloud deck. Given the circumstances what has been inferred to date about the large-scale trans

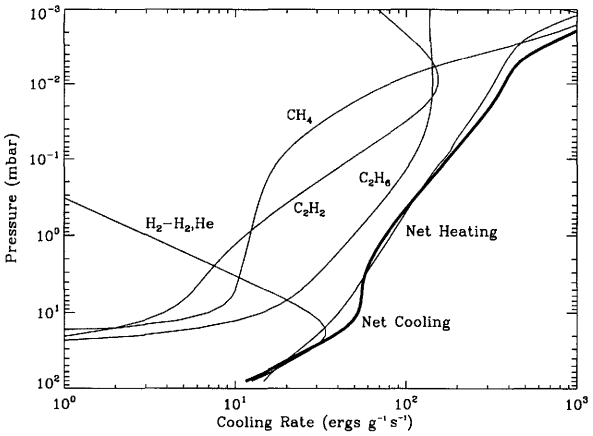

Figure 7.6. Net stratospheric heating and cooling rates calculated in the radiative equilibrium model of Yelle *et al.* 2001. The contributions of the different thermal infrared bands to the net cooling are also shown (as marked). Ethane is the primary coolant throughout much of the stratosphere, whereas methane dominates at high altitudes. Cooling rates expressed in K s^{-1} can be obtained by dividing the above cooling rate by $\sim 1.3 \times 10^8$.

port has been derived mainly by examining the steady, two-dimensional, longitudinally averaged momentum and thermodynamic energy budgets of the stratosphere. In these two-dimensional models, longitudinally averaged transport by the three-dimensional circulation is parameterized in terms of an advective meridional circulation and eddy diffusion coefficients. Consideration of the momentum and energy budgets then allows calculation of the residual-mean meridional circulation, which approximates the advective portion of the total transport when eddies are small-amplitude, statistically steady, and adiabatic (Andrews *et al.* 1987). If, in addition to these conditions, the tracer is conserved following the motion of fluid parcels, then the entire mass transport is represented by the advection term. Tracer dispersion arising from eddy transience, nonlinear eddy-eddy interactions, or "chemical diffusion" is represented in two-dimensional models in the form of eddy diffusion.

Gierasch *et al.* (1986) deduced the two-dimensional residual mean meridional circulation at the 150- and 270-mbar pressure levels based on an analysis of *Voyager* IRIS data. The meridional circulation was calculated using a simple axisymmetric dynamical model in which Coriolis acceleration of the zonal wind is balanced by a linear mechanical drag and in which radiative diabatic heating is balanced by adiabatic cooling. Upwelling was found to occur above anticyclonic zones and subsidence to occur above cyclonic belts. The observed variations with latitude of the 45-μm cloud optical depth, ammonia abundance, and para hydrogen fraction were found to be consistent with concentration by upward vertical motion above the zones, suggesting that the residual circulation near the tropopause closely approximates the effective transport circulation. Later, Conrath *et al.* (1990) extended calculation of the residual circulation up to the 0.1-mbar pressure level, using a similar dynamical model but including seasonally varying insolation. Their circulation took the same form as that of Gierasch *et al.* (1986) below the ~10-mbar level, with regions of upwelling and subsidence alternating with latitude over zones and belts. Above the ~10-mbar level, this circulation gave way to a global gyre with rising motion over the equator and subsidence over the poles.

Conrath *et al.* (1990) ignored the effect of solar heating due to aerosol absorption, which is strongest in the polar regions and has important implications for the residual circulation. West *et al.* (1992) used improved band parameters to calculate energy deposition in CH_4 and paid particular attention to aerosols. Observations from IUE and *Voyager* were used to determine the aerosol distribution as a function of latitude. Cooling from C_2H_2 and C_2H_6 emissions was included but the C_2H_2 and C_2H_6 distributions were assumed to be constant with latitude and altitude. They inferred a residual circulation that differed fundamentally from that of Conrath *et al.* (1990) and consisted of a two-cell structure in each hemisphere centered near the 10-mbar level, with subsidence occurring at low and mid latitudes and upwelling at high latitudes. Air lying above ~10 mbar drifts equatorward in this model while air below this level drifts poleward. Below the ~100-mbar level, their circulation is similar to that obtained by Gierasch *et al.* (1986) for the upper troposphere, but with the important difference that strong subsidence is predicted for regions poleward of ±50°. This subsidence is induced by net radiative cooling of the upper troposphere in the polar regions. Moreno and Sedano (1997) also calculated a residual circulation using the methods of West *et al.* (1992), but inferred a different spatial distribution for the stratospheric aerosol and related solar heating. They obtained a markedly different circulation above the ~50-mbar level, with upwelling at low and mid latitudes and subsidence at high latitudes, except for a small region of upwelling at high altitudes in the southern polar region; air parcels drift from equator to pole in each hemisphere. Below the ~50-mbar level, their residual circulation is qualitatively similar to that of West *et al.* (1992), with poleward drift at middle to high latitudes in both hemispheres.

As is discussed by Yelle *et al.* (2001), photochemical species play a critical role in the energy balance of the jovian stratosphere. The results shown in Fig. 7.6 show that C_2H_6 is the dominant coolant in the stratosphere over a broad region from 0.2 to 20 mbar. The dominance of C_2H_6 cooling has previously been unappreciated, and, as a consequence, studies of stratospheric dynamics to date have ignored latitudinal variations in the abundance of photochemical constituents like C_2H_6. The latitudinal variations of both ethane and acetylene should be included in future models of stratospheric dynamics (see Section 7.2.3 and 7.2.7 for further discussion of the latitude profiles of C_2H_2 and C_2H_6).

All of the above models for the residual circulation predict a general poleward drifting of air between the 100- and 10-mbar levels. On the other hand, observations of the spreading of aerosol impact debris in the lower stratosphere during the ~3 years following the collision of comet SL9 with Jupiter indicated relatively rapid equatorward transport from the impact latitude at 45° S to at least as far as 20° S (West 1996, Sanchez-Lavega *et al.* 1998, Friedson *et al.* 1999). The transport predicted by the residual circulation models is inconsistent with these observations; it is in the wrong direction in the lower stratosphere and is much too slow. This discrepancy led Friedson *et al.* (1999) to propose

an alternative, phenomenological model for the transport, in which transient and/or nonlinear effects (such as wave breaking) in large-scale quasi-geostrophic eddies act as the principal agent for mixing the stratosphere. This type of mixing is parameterized in two-dimensional models in terms of a latitudinal eddy diffusion coefficient, K_{yy}. By estimating the flux–gradient ratio of northward potential vorticity transport below the 10-mbar level, Friedson *et al.* derived a map of the annually averaged K_{yy} for the jovian stratosphere. They found $K_{yy} \sim 10^{11}$ cm^2 s^{-1} near the poles in each hemisphere, decreasing more or less monotonically to values less than 10^{10} cm^2 s^{-1} at low latitudes.

The latitudinal gradient of K_{yy} inferred by Friedson *et al.* (1999) is particularly notable since it promotes steady equatorward transport of quasi-conservative tracers at low and middle latitudes in Jupiter's lower stratosphere. In the transport equation, the gradient of K_{yy} behaves as an effective equatorward velocity that at certain latitudes dominates that associated with the residual circulation. The net effect is then the prediction of relatively large equatorward transport in the lower stratosphere in both hemispheres. Friedson *et al.* (1999) introduced their derived K_{yy} into a two-dimensional dynamical transport model and found that the predicted rate of equatorward spreading of SL9 impact debris agreed well with that derived from the observations, suggesting that their K_{yy} provides a useful first-order description of mean eddy transport in the lower stratosphere at low and middle southern latitudes. It remains to be seen whether this model produces as accurate a description of transport for other species and latitudes as it did for SL9 debris in the southern hemisphere. The role of feedback between the meridional transport and active radiative cooling by C_2H_2 and C_2H_6 needs further investigation.

The observations of the SL9 aerosols pertain to the lower stratosphere below ~10 mbar. K_{yy} might also vary with altitude in the upper stratosphere. In a simple two-dimensional model designed to simulate the horizontal spreading of high-altitude CO and CO_2 vapors that were deposited after the SL9 impacts, Lellouch *et al.* (2002) found that a latitude-independent value of $K_{yy} = 2 \times 10^{11}$ cm^2 s^{-1} in the ~0.2–0.5-mbar region allowed the observed variation of CO and CO_2 to be reproduced for the first several years following the impacts. Note, however, that the spatial resolution for the vapor observations was much worse than that of the aerosol observations, and latitudinally dependent K_{yy} profiles remain to be investigated.

The calculation of transport in two-dimensional models is based by necessity on a number of assumptions, not all of which may be valid. A more rigorous approach entails mapping the quasi-geostrophic potential vorticity on isentropic surfaces, a technique that has provided great insight into the nature of transport in the terrestrial stratosphere (McIntyre and Palmer 1984, Leovy *et al.* 1985). This approach requires large amounts of data concerning the three-dimensional temperature field in the stratosphere. These data are presently unavailable for Jupiter but may become available for Saturn's stratosphere after the *Cassini* mission.

7.6 SUMMARY AND CONCLUSIONS

Our understanding of the composition, chemistry, thermal structure, and dynamics of the jovian stratosphere has improved tremendously since the first *Pioneer* spacecraft encounters with Jupiter in 1973 and 1974. Four additional spacecraft flybys (*Voyager 1* and *2*, *Ulysses*, and now *Cassini*), an orbiting spacecraft and in situ atmospheric probe (*Galileo*), and numerous Earth-based observations have provided a wealth of new information about the jovian system. The jovian stratosphere is known to contain mostly hydrogen and helium, with 0.18% methane by volume, and trace amounts of other hydrocarbon and oxygen compounds (e.g., CH_3, C_2H_2, C_2H_4, C_2H_6, CH_3C_2H, C_4H_2, C_6H_6, CO, H_2O, and CO_2 have been definitively identified). Stratospheric constituents with abundances as low as a part per billion are now routinely detected. As on the Earth, many of these trace species (particularly CH_4, C_2H_6, and C_2H_2) are critical in controlling atmospheric temperatures. Methane photochemistry appears to dominate the production of the disequilibrium hydrocarbons. One-dimensional photochemical models are able to reproduce the observed CH_4, C_2H_6, and C_2H_2 abundances but tend to underpredict the abundances of some of the heavier species (e.g., CH_3C_2H and C_6H_6). Part of the problem lies with the lack of appropriate laboratory data at the temperatures, pressures, and other conditions relevant to the jovian stratosphere. The detection of stratospheric H_2O, CO, and CO_2 indicates that Jupiter is receiving material from outside its atmosphere, most likely from comets, but also from interplanetary dust and from the planet's satellite and ring systems. As was indicated by the Shoemaker–Levy 9 impacts with Jupiter and by continuing observations of oxygen, nitrogen, and sulfur compounds in the jovian stratosphere, this external material can affect stratospheric composition over timescales both short and long.

Stratospheric temperatures and composition are now known to be intimately connected. Temperatures increase from the tropopause into the stratosphere due to absorption of solar radiation in the near-infrared bands of methane. Stratospheric cooling occurs mainly through radiative emissions in the mid- and far-infrared bands of CH_4, C_2H_6, and C_2H_2. The dramatic increase in temperatures at the top of the stratosphere is most likely tied to the relatively abrupt decrease in hydrocarbon abundances at high altitudes as these molecules become diffusively separated. Spatial variations in vapor and aerosol abundances affect radiative heating and cooling rates and can drive stratospheric dynamics. Temperatures have been measured at all pressures in the stratosphere, but complete three-dimensional information is not yet available. Small- and large-scale perturbations in the temperature profile indicate the presence of atmospheric waves or other dynamical features. The vapor and aerosol debris deposited in the jovian stratosphere after the Shoemaker–Levy 9 impacts have fortuitously provided tracers from which stratospheric circulation patterns can be inferred. Observations of the SL9 debris indicate a generally equatorward drift of air in the stratosphere, a conclusion that is at odds with the predictions of transport by the residual circulations calculated with current models.

Many questions remain with regard to stratospheric composition and chemistry. We still do not know the majo

chemical pathways that lead to the production of complex hydrocarbons (i.e., more than 3 carbon atoms) and aerosol in the jovian stratosphere. What are the relative roles of photochemistry and auroral chemistry? Is ion chemistry important? What processes determine the distribution of chemical constituents throughout the stratosphere of Jupiter? Is dynamics important? Even the chemistry of simple hydrocarbons is not well constrained, as the branching ratios of CH_4 photolysis at Lyman α are not known. Our understanding of stratospheric chemistry would be greatly improved if we had more laboratory data on kinetic reaction rate coefficients and products, ultraviolet absorption cross sections, and photolysis quantum yields for relevant hydrocarbons at appropriate temperatures and pressures. Experimental data on ion-molecule reactions are also needed to better understand chemistry in the auroral regions.

Observations that constrain the vertical distribution of the different stratospheric constituents would provide useful information about the strength of atmospheric mixing and the effectiveness of different chemical production and loss mechanisms in Jupiter's stratosphere. Observations that more accurately constrain the decrease in methane mole fraction with decreasing pressure in the upper stratosphere are particularly needed because such information provides critical clues to understanding both hydrocarbon photochemistry and stratospheric radiative processes. Does the methane homopause level vary with location and time? Spatially resolved observations are also becoming increasingly important for improving our understanding of transport processes and for addressing such issues as how auroral chemistry affects the global stratospheric composition and haze production rates. Does photochemistry or transport dominate the observed variation of hydrocarbons with latitude? Two- or three-dimensional photochemical models may now be needed to resolve this issue.

Chemical models would also be better constrained by new detections or better upper limits for trace species like CH_3 in non-auroral regions, and C_3H_8, C_3H_6, CH_2CCH_2, C_4H_{10}, C_4H_4, and C_4H_6 in both auroral and non-auroral regions. Given the similarities and differences in the stratospheric compositions of all the giant planets, theoretical models must be developed that present a consistent picture of hydrocarbon chemistry on all the giant planets and that address the reasons for the similarities and differences among planets. Observations of the spatial distribution of H_2O in the jovian stratosphere would confirm or refute the suggestion that the H_2O and CO_2 that are currently observed derive mainly from the SL9 impacts. If possible, the stratospheric CO, CO_2, and H_2O abundances should be monitored to track variations with time. Such information would help constrain the origin and influx rate of external material to the giant planets and would have important implications for our understanding of the exchange of material in the outer solar system. Searches for other non-native stratospheric species (such as metals or sulfur-bearing compounds) might also help constrain the influx rate of extraplanetary material. Some of the observational data discussed above will be supplied by the analysis of the *Cassini* flyby data (especially data from the CIRS and UVIS instruments); other information will require Earth-based observations or future spacecraft missions.

Our knowledge and understanding of the stratospheric thermal structure and dynamics is also not complete. What is the three-dimensional structure of atmospheric temperatures? Do processes besides radiative heating and cooling affect average temperatures? How do atmospheric waves influence transport and temperatures? How does ortho/para H_2 interconversion occur, and how does it affect the thermal structure? How and why does the stratospheric thermal structure vary with time? What drives the dynamics of the jovian stratosphere? How significant is meridional transport in affecting concentrations of trace species in the stratosphere? What is the nature of tracer transport at altitudes above the ~1-mbar pressure level? Does the QQO affect tracer transport and chemistry at low latitudes? To answer these and other questions, we will need to gather global information on the spatial distribution of temperatures and hydrocarbon abundances and tie this information into more sophisticated theoretical models. Advances in detector technology may allow us to gather direct information on wind velocities in the stratosphere through measurement of Doppler shifts in line profiles. Theoretical models would also benefit from new laboratory data. Measurements of the collisional deactivation rates for hydrocarbons (especially CH_3, C_2H_2, C_2H_4, and C_2H_6) by H_2 and He at low temperatures would improve thermal models, as a significant portion of the infrared emission comes from sub-microbar pressure levels where non-local thermodynamic equilibrium effects might be important. The lack of a detailed near-infrared CH_4 absorption spectrum for appropriate conditions constitutes a source of significant uncertainty in calculations of stratospheric heating rates. Further progress will occur from a synergistic combination of new observations, theory, and laboratory measurements.

The stratosphere is one of the most accessible regions of the jovian atmosphere as far as remote sensing observations are concerned. Although we have learned a lot in the past few decades, much remains unknown. Further study into the chemical and physical processes that operate in the jovian stratosphere can teach us about similar processes that occur in the atmospheres of other planets, including Earth. We must better understand the composition, thermal structure, and dynamics of Jupiter and the other giant planets in our own solar system before we can hope to understand or predict the properties of extrasolar giant planets and substellar companions that now are being discovered at a prodigious rate. The *Cassini* flyby promises to deliver much useful information about the jovian stratosphere, and advances in Earth-based telescope technology will provide still more. Ultimately, to better understand stratospheric behavior in the auroral regions and to understand global meridional variability, a polar orbiting spacecraft would be ideal.

REFERENCES

Ajello, J., D. Shemansky, W. Pryor, K. Tobiska, C. Hord, S. Stephens, I. Stewart, J. Clarke, K. Simmons, W. McClintock, C. Barth, J. Gebben, D. Miller, and B. Sandel, *Galileo* orbiter ultraviolet absorption of Jupiter aurora, *J. Geophys. Res.* **103**, 20 125–20 148, 1998.

Allen, M., J. P. Pinto, and Y. L. Yung, Titan: Aerosol photochemistry and variations related to the sunspot cycle, *ApJ* **242**, L125–L128, 1980.

Allen, M., Y. L. Yung, and G. R. Gladstone, The relative abundance of ethane to acetylene in the jovian stratosphere, *Icarus* **100**, 527–533, 1992.

Allen, M., Y.-T. Lee, A. Friedson, G. Orton, and R. West, Transport in the jovian stratosphere: Insight from a 2D model of ethane, *BAAS* **32**, 1008, 2000.

Allen, M., A. Y. T. Lee, E. Serabyn, and E. W. Weisstein, Vertical transport in the jovian upper troposphere: Insights from phosphine submillimeter observations, *BAAS* **33**, 1042, 2001.

Allison, M., Planetary waves in Jupiter's equatorial atmosphere, *Icarus* **83**, 282–307, 1990.

Andrews, D. G., J. R. Holton, and C. B. Leovy, *Middle Atmospheric Dynamics*, Academic Press, 1987.

Anicich, V. G., D. B. Milligan, D. A. Fairley, and M. J. McEwan, Termolecular ion–molecule reactions in Titan's atmosphere: I. Principal ions with principal neutrals, *Icarus* **146**, 118–124, 2000.

Appleby, J. F., CH_4 nonlocal thermodynamic equilibrium in the atmospheres of the giant planets, *Icarus* **85**, 355–379, 1990.

Appleby, J. F. and J. S. Hogan, Radiative–convective equilibrium models of Jupiter and Saturn, *Icarus* **59**, 336–366, 1984.

Atreya, S. K., *Atmospheres and Ionospheres of the Outer Planets and Their Satellites*, Springer-Verlag, 1986.

Atreya, S. K. and T. M. Donahue, Models of the jovian upper atmosphere, *Rev. Geophys. Space Phys.* **17**, 388–396, 1979.

Atreya, S. K., T. M. Donahue, B. R. Sandel, A. L. Broadfoot, and G. R. Smith, Jovian upper atmospheric temperature measurement by the *Voyager 1* UV spectrometer, *Geophys. Res. Lett.* **6**, 795–798, 1979.

Atreya, S. K., T. M. Donahue, and M. C. Festou, Jupiter: Structure and composition of the upper atmosphere, *ApJ* **247**, L43–L47, 1981.

Atreya, S. K., J. H. Waite, Jr., T. M. Donahue, A. F. Nagy, and J. C. McConnell, Theory, measurements, and models of the upper atmosphere and ionosphere of Saturn, in *Saturn*, T. Gehrels, M.S. Matthews (eds), University of Arizona Press, pp. 239–277, 1984.

Beebe, R. F., G. S. Orton, and R. A. West, Time-variable nature of the jovian cloud properties and thermal structure: An observational perspective, in *Time-Variable Phenomena in the Jovian System*, M. J. S. Belton, R. A. West, and J. Rahe, eds, pp. 245–296, NASA SP-494, 1989.

Beer, R., Detection of carbon monoxide in Jupiter, *ApJ* **200**, L167–L169, 1975.

Beer, R. and F. Taylor, The abundance of carbon monoxide in Jupiter, *ApJ* **221**, 1100–1109, 1978.

Beer, R. and F. W. Taylor, Comment on "Carbon monoxide in Jupiter after Comet Shoemaker–Levy 9," by K. S. Noll, D. Gilmore, R. F. Knacke, M. Womack, C. A. Griffith, and G. Orton, *Icarus* **133**, 321, 1998.

Ben Jaffel, L., C. Magnan, and A. Vidal-Madjar, The Lyman alpha albedo of Jupiter, *A&A* **204**, 319–326, 1988.

Ben Jaffel, L., V. Leers, and B. R. Sandel, Dark auroral oval on Saturn discovered in Hubble Space Telescope ultraviolet images, *Science* **269**, 951–953, 1995.

Bergin, E. A., E. Lellouch, M. Harwit, M. A. Gurwell, G. J. Melnick, M. L. N. Ashby, G. Chin, N. R. Erickson, P. F. Goldsmith, J. E. Howe, S. C. Kleiner, D. G. Koch, D. A. Neufeld, B. M. Patten, R. Plume, R. Schieder, R. L. Snell, J. R. Stauffer, V. Tolls, Z. Wang, G. Winnewisser, and Y. F. Zhang, Submillimeter Wave Astronomy Satellite observations of Jupiter and Saturn: Detection of 557 GHz water emission, *ApJ* **539**, L147–L150, 2000.

Bétremieux, Y. and R. V. Yelle, HST detection of H_2 Raman scattering in the jovian atmosphere, *Icarus* **142**, 324–341, 1999.

Bezanger, C., B. Bézard, and D. Gautier, Spatial variation of the thermal structure of Jupiter's atmosphere, in *The Jovian Atmospheres*, M. A. Allison and L. D. Travis, eds, pp. 79–81, NASA Conf. Publ. 2441, 1986.

Bézard, B., Long-term response of Jupiter's thermal structure to the SL9 impacts, *Planet. Space Sci.* **45**, 1251–1270, 1997.

Bézard, B., C. Griffith, J. Lacy, and T. Owen, Non-detection of hydrogen cyanide on Jupiter, *Icarus* **118**, 384–391, 1995.

Bézard, B., C. A. Griffith, D. M. Kelly, J. H. Lacy, T. Greathouse, and G. Orton, Thermal infrared imaging spectroscopy of Shoemaker–Levy 9 impact sites: Temperature and HCN retrievals, *Icarus* **125**, 94–120, 1997.

Bézard, B., P. Drossart, T. Encrenaz, and H. Feuchtgruber, Benzene on the giant planets, *Icarus* **154**, 492–500, 2001a.

Bézard, B., J. I. Moses, J. Lacy, T. Greathouse, M. Richter, and C. Griffith, Detection of ethylene C_2H_4 on Jupiter and Saturn in non-auroral regions, *BAAS* **33**, 1079–1080, 2001b.

Bézard, B., E. Lellouch, D. Strobel, J.-P. Maillard, and P. Drossart, Carbon monoxide on Jupiter: Evidence for both internal and external sources, *Icarus* **159**, 95–111, 2002.

Billebaud, F., P. Drossart, I. Vauglin, P. Merlin, F. Sibille, P. Lognonné, E. Lellouch, and B. Mosser, 10 micron mapping of Jupiter on the CFHT after the impacts of Comet P/Shoemaker–Levy 9, *Geophys. Res. Lett.* **22**, 1777–1780, 1995.

Bjoraker, G. L., H. P. Larson, and V. G. Kunde, The gas composition of Jupiter derived from 5-μm airborne spectroscopic observations, *Icarus* **66**, 579–609, 1986.

Bottke, Jr., W. F., A. Morbidelli, R. Jedicke, J. Petit, H. F. Levison, P. Michel, and T. S. Metcalfe, Debiased orbital and absolute magnitude distribution of the Near-Earth Objects, *Icarus* **157**, 399–433, 1986.

Broadfoot, A. L., M. J. Belton, P. Z. Takacs, B. R. Sandel, D. E. Shemansky, J. B. Holberg, J. M. Ajello, H. W. Moos, S. K. Atreya, T. M. Donahue, J. L. Bertaux, J. E. Blamont, D. F. Strobel, J. C. McConnell, R. Goody, A. Dalgarno, and M. B. McElroy, Extreme ultraviolet observations from *Voyager 1* encounter with Jupiter, *Science* **204**, 979–982, 1979.

Broadfoot, A. L., B. R. Sandel, D. E. Shemansky, J. C. McConnell, G. R. Smith, J. B. Holberg, S. K. Atreya, T. M. Donahue, D. F. Strobel, and J. L. Bertaux, Overview of the *Voyager* ultraviolet spectrometry results through Jupiter encounter, *J. Geophys. Res.* **86**, 8259–8284, 1981.

Brownsword, R. A., M. Hillenkamp, T. Laurent, R. K. Vasta, H.-R. Volpp, and J. Wolfrum, Quantum yield of H atom formation in the methane dissociation after photoexcitation at the Lyman-α (121.6 nm) wavelength, *Chem. Phys. Lett.* **266**, 259–266, 1997.

Cadle, R. D., The photochemistry of the upper atmosphere of Jupiter, *J. Atmos. Sci.* **19**, 281–285, 1962.

Caldwell, J., A. T. Tokunaga, and F. C. Gillett, Possible infrared aurorae on Jupiter, *Icarus* **44**, 667–675, 1980.

Caldwell, J., A. T. Tokunaga, and G. S. Orton, Further observations of 8-μm polar brightenings of Jupiter, *Icarus* **53**, 133–140, 1983.

Caldwell, J., R. Halthore, G. Orton, and J. Bergstralh, Infrared polar brightenings on Jupiter: IV. Spatial properties of methane emission, *Icarus* **74**, 331–339, 1988.

Carlson, R. W. and D. L. Judge, The extreme ultraviolet dayglow of Jupiter, *Planet. Space Sci.* **19**, 327–343, 1971.

Cess, R. D. and S. C. Chen, The influence of ethane and acetylene upon the thermal structure of the jovian atmosphere, *Icarus* **26**, 444–450, 1975.

Cess, R. D. and S. Khetan, Radiative transfer within the atmospheres of the major planets, *J. Quant. Spectrosc. Radiativ Transf.* **13**, 995–1009, 1973.

Clarke, J. T., H. W. Moos, and P. D. Feldman, The far-ultraviolet spectra and geometric albedos of Jupiter and Saturn, *Ap* **255**, 806–818, 1982.

Clarke, J. T., R. Gladstone, W. Pryor, J. Ajello, L. Ben Jaffel, J. Connerney, J. C. Gerard, J. Trauger, and H. Wait

HST/STIS observations of a dawn auroral storm on Jupiter, *BAAS* **32**, 1012, 2000.

Combes, M., T. Encrenaz, L. Vapillon, Y. Zéau, and C. Lesqueren, Confirmation of the identification of C_2H_2 and C_2H_6 in the jovian atmosphere, *A&A* **34**, 33–35, 1974.

Conrath, B. J. and D. Gautier, Saturn helium abundance: A reanalysis of *Voyager* measurements, *Icarus* **144**, 124–134, 2000.

Conrath, B. J. and P. J. Gierasch, Global variation of para hydrogen fraction in Jupiter's atmosphere and implications for dynamics on the outer planets, *Icarus* **57**, 184–204, 1984.

Conrath, B. J., P. J. Gierasch, and N. Nath, Stability of zonal flows on Jupiter, *Icarus* **48**, 256–282, 1981.

Conrath, B. J., D. Gautier, R. A. Hanel, and J. S. Hornstein, The helium abundance on Saturn from *Voyager* measurements, *ApJ* **282**, 807–815, 1984.

Conrath, B. J., P. J. Gierasch, and S. S. Leroy, Temperature and circulation in the stratosphere of the outer planets, *Icarus* **83**, 255–281, 1990.

Deming, D., M. J. Mumma, F. Espenak, D. E. Jennings, T. Kostiuk, G. Wiedemann, R. Loewenstein, and J. Piscitelli, A search for p-mode oscillations of Jupiter: Serendipitous observations of nonacoustic thermal wave structure, *ApJ* **343**, 456–467, 1989.

Deming, D., D. Reuter, D. Jennings, G. Bjoraker, G. McCabe, K. Fast, and G. Wiedemann, Observations and analysis of longitudinal thermal waves on Jupiter, *Icarus* **126**, 301–312, 1997.

Dols, V., J.-C. Gérard, J. T. Clarke, J. Gustin, and D. Grodent, Diagnostics of the jovian aurora deduced from ultraviolet spectroscopy: Model and HST/GHRS observations, *Icarus* **147**, 251–266, 2000.

Drossart, P., B. Bézard, S. Atreya, J. Lacy, E. Serabyn, A. Tokunaga, and T. Encrenaz, Enhanced acetylene emission near the north pole of Jupiter, *Icarus* **66**, 610–618, 1986.

Drossart, P., B. Bézard, S. K. Atreya, J. Bishop, J. H. Waite, Jr., and D. Boice, Thermal profiles in the auroral regions of Jupiter, *ApJ* **98**, 18 803–18 811, 1993a.

Drossart, P., J.-P. Maillard, J. Caldwell, and J. Rosenqvist, Line-resolved spectroscopy of the jovian H_3^+ auroral emission at 3.5 micrometers, *ApJ* **402**, L25–L28, 1993b.

Drossart, P., T. Fouchet, J. Crovisier, E. Lellouch, T. Encrenaz, H. Feuchtgruber, and J.-P. Champion, Fluorescence in the 3 micron bands of methane on Jupiter and Saturn from ISO/SWS observations, in *The Universe as Seen by ISO*, P. Cox and M. F. Kessler, eds, pp. 169–172, ESA SP-427, 1999.

Drossart, P., B. Sicardy, F. Roques, T. Widemann, G. R. Gladstone, J. H. Waite, and M. Vincent, The methane homopause of Jupiter as seen in IR spectroscopy from the occultation of star HIP9369, *BAAS* **32**, 1013, 2000.

Drossart, P., T. Fouchet, E. Raynaud, B. Sicardy, T. Widemann, J. H. Waite, and G. R. Gladstone, The upper atmosphere of Jupiter from VLT/ISAAC observations, *BAAS* **33**, 1026, 2001.

Edgington, S. G., S. K. Atreya, L. M. Trafton, J. J. Caldwell, R. F. Beebe, A. A. Simon, R. A. West, and C. Barnet, On the latitude variation of ammonia, acetylene, and phosphine altitude profiles on Jupiter from HST Faint Object Spectrograph observations, *Icarus* **133**, 192–209, 1998.

Edgington, S. G., S. K. Atreya, L. M. Trafton, J. J. Caldwell, R. F. Beebe, A. A. Simon, and R. A. West, Ammonia and eddy mixing variations in the upper troposphere of Jupiter from HST Faint Object Spectrograph observations, *Icarus* **142**, 342–356, 1999.

Edgington, S. G., R. A. West, A. J. Friedson, and S. K. Atreya, A 2-D photochemical model with meridional circulation, *BAAS* **32**, 1013, 2000.

Emerich, C., L. Ben Jaffel, and R. Prangé, On the analysis of the H Lyman-α dayglow of Jupiter Saturn and Uranus, *Planet. Space Sci.* **41**, 363–371, 1993.

Encrenaz, T., T. de Graauw, S. Schaeidt, E. Lellouch, H. Feuchtgruber, D. A. Beintema, B. Bézard, P. Drossart, M. Griffin, A. Heras, M. Kessler, K. Leech, P. Morris, P. R. Roelfsema, M. Roos-Serote, A. Salama, B. Vandenbussche, E. A. Valentijn, G. R. Davis, and D. A. Naylor, First results of ISO–SWS observations of Jupiter, *A&A* **315**, L397–L400, 1996.

Fahr, A., P. S. Monks, L. J. Stief, and A. H. Laufer, Experimental determination of the rate constant for the reaction of C_2H_3 with H_2 and implications for the partitioning of hydrocarbons in the atmospheres of the outer planets, *Icarus* **116**, 415–422, 1995.

Feldman, P. D., M. A. McGrath, H. W. Moos, S. T. Durrance, D. F. Strobel, and A. F. Davidsen, The spectrum of the jovian dayglow observed at 3 Å resolution with the Hopkins Ultraviolet Telescope, *ApJ* **406**, 279–284, 1993.

Festou, M. C., S. K. Atreya, T. M. Donahue, B. R. Sandel, D. E. Shemansky, and A. L. Broadfoot, Composition and thermal profiles of the jovian upper atmosphere determined by the *Voyager* ultraviolet stellar occultation experiment, *J. Geophys. Res.* **86**, 5715–5725, 1981.

Feuchtgruber, H., E. Lellouch, T. de Graauw, B. Bézard, T. Encrenaz, and M. Griffin, External supply of oxygen to the atmospheres of the giant planets, *Nature* **389**, 159–162, 1997.

Feuchtgruber, H., E. Lellouch, T. Encrenaz, B. Bézard, A. Coustenis, P. Drossart, A. Salama, T. de Graauw, and G. R. Davis, Oxygen in the stratospheres of the giant planets and Titan, in *The Universe as Seen by ISO*, P. Cox and M. F. Kessler, eds, pp. 133–136, ESA SP-427, 1999.

Flasar, F. M., Temporal behavior of Jupiter's meteorology, in *Time-Variable Phenomena in the Jovian System*, M. J. S. Belton, R. A. West, and J. Rahe, eds, pp. 324–343, NASA SP-494, 1989.

Flasar, F. M., A. A. Simon-Miller, R. K. Achterberg, B. J. Conrath, P. J. Gierasch, V. G. Kunde, C. Nixon, D. E. Jennings, P. N. Romani, P. Irwin, B. Bezard, R. Carlson, and *Cassini* CIRS Investigation Team, Prospecting Jupiter in the thermal infrared with *Cassini* CIRS: Atmospheric temperatures and dynamics, *BAAS* **33**, 1025, 2001.

Flasar, F. M., V. G. Kunde, C. Nixon, G. L. Bjoraker, D. E. Jennings, P. N. Romani, A. A. Simon-Miller, R. K. Achterberg, B. K. Conrath, P. J. Gierasch, B. Bézard, P. Irwin, R. Carlson, G. Orton, L. Spilker, S. Edberg, J. Brasunas, J. C. Pearl, M. Smith, S. Calcutt, P. Read, F. Taylor, T. Fouchet, A. Barucci, A. Coustenis, R. Courtin, D. Gautier, E. Lellouch, A. Marten, C. Ferrari, R. Prangé, T. Owen, M. Abbas, R. E. Samuelson, F. Raulin, P. Ade, C. Cesarsky, K. Grossman, and A. Coradini, CIRS at Jupiter: An overview of atmospheric temperatures and composition, in *Jupiter after Galileo and Cassini*, International Symposium, Lisbon, Portugal, 2002.

Fouchet, T., E. Lellouch, B. Bézard, H. Feuchtgruber, P. Drossart, and T. Encrenaz, Jupiter's hydrocarbons observed with ISO–SWS: Vertical profiles of C_2H_6 and C_2H_2, detection of CH_3C_2H, *A&A* **355**, L13–L17, 2000.

Fouchet, T., E. Lellouch, and H. Feuchtgruber, The hydrogen ortho-to-para ratio in the stratospheres of the giant planets, *Icarus* **161**, 127–143, 2002.

Friedson, A. J., New observations and modeling of a QBO-like oscillation in Jupiter's stratosphere, *Icarus* **137**, 34–55, 1999.

Friedson, A. J., R. A. West, A. K. Hronek, N. A. Larsen, and N. Dalal, Transport and mixing in Jupiter's stratosphere inferred from comet S–L9 dust migration, *Icarus* **138**, 141–156, 1999.

Friedson, A. J., A.-S. Wong, and Y. L. Yung, Models for polar haze formation in Jupiter's stratosphere, *Icarus* **158**, 389–400, 2002.

Gautier, D. and R. Courtin, Atmospheric thermal structures of the giant planets, *Icarus* **39**, 28–45, 1979.

Gautier, D. and I. Revah, Sounding of planetary atmospheres: A Fourier analysis of the radiative transfer equation, *J. Atmos. Sci.* **32**, 881–892, 1975.

Gautier, D., B. Conrath, M. Flasar, R. Hanel, V. Kunde, A. Chedin, and N. Scott, The helium abundance of Jupiter from *Voyager*, *J. Geophys. Res.* **86**, 8713–8720, 1981.

Gautier, D., B. Bézard, A. Marten, J. P. Baluteau, N. Scott, A. Chedin, V. Kunde, and R. Hanel, The C/H ratio in Jupiter from the *Voyager* infrared investigation, *ApJ* **257**, 901–912, 1982.

Gérard, J. C., V. Dols, D. Grodent, J. H. Waite, G. R. Gladstone, and R. Prangé, Simultaneous observations of the saturnian aurora and polar haze with the HST/FOC, *Geophys. Res. Lett.* **22**, 2685–2688, 1995.

Gierasch, P. J., B. J. Conrath, and J. A. Magalhães, Zonal mean properties of Jupiter's upper troposphere from *Voyager* infrared observations, *Icarus* **67**, 456–483, 1986.

Gillett, F. C. and J. A. Westphal, Observations of 7.9-micron limb brightening on Jupiter, *ApJ* **179**, L153–L154, 1973.

Gillett, F. C., F. J. Low, and W. A. Stein, The 2.8–14-micron spectrum of Jupiter, *ApJ* **157**, 925–934, 1969.

Gladstone, G. R. and Y. L. Yung, An analysis of the reflection spectrum of Jupiter from 1500 Å to 1740 Å, *ApJ* **266**, 415–424, 1983.

Gladstone, G. R., D. T. Hall, and Waite, J. H., Jr., EUVE observations of Jupiter during the impact of Comet Shoemaker–Levy 9, *Science* **268**, 1595–1597, 1995.

Gladstone, G. R., M. Allen, and Y. L. Yung, Hydrocarbon photochemistry in the upper atmosphere of Jupiter, *Icarus* **119**, 1–52, 1996.

Gladstone, G. R., J. H. Waite, D. Grodent, W. S. Lewis, F. J. Crary, R. F. Elsner, M. C. Weisskopf, T. Majeed, J.-M. Jahn, A. Bhardwaj, J. T. Clarke, D. T. Young, M. K. Dougherty, S. A. Espinosa, and T. E. Cravens, A pulsating auroral x-ray hot spot on Jupiter, *Nature* **415**, 1000–1003, 2002.

Grodent, D., J. H. Waite, Jr., and J.-C. Gérard, A self-consistent model of the jovian auroral thermal structure, *J. Geophys. Res.* **106**, 12 933–12 952, 2001.

Halthore, R., A. Burrows, and J. Caldwell, Infrared polar brightenings on Jupiter: V. A thermal equilibrium model for the north polar hot spot, *Icarus* **74**, 340–350, 1988.

Hanel, R., B. Conrath, M. Flasar, L. Herath, V. Kunde, P. Lowman, W. Maguire, J. Pearl, J. Pirraglia, and L. Horn, Infrared observations of the jovian system from *Voyager 2*, *Science* **206**, 952–956, 1979a.

Hanel, R., B. Conrath, M. Flasar, V. Kunde, P. Lowman, W. Maguire, J. Pearl, J. Pirraglia, R. Samuelson, D. Gautier, P. Gierasch, S. Kumar, and C. Ponnamperuma, Infrared observations of the jovian system from *Voyager 1*, *Science* **204**, 972–976, 1979b.

Heck, A. J. R., R. N. Zare, and D. W. Chandler, Photofragment imaging of methane, *J. Chem. Phys.* **104**, 4019–4030, 1996.

Hogan, J. S., S. I. Rasool, and T. E. Encrenaz, The thermal structure of the jovian atmosphere, *J. Atmos. Sci.* **26**, 898–905, 1969.

Hubbard, W. B., V. Haemmerle, C. C. Porco, G. H. Rieke, and M. J. Rieke, The occultation of SAO 78505 by Jupiter, *Icarus* **113**, 103–109, 1995.

Hunten, D. M., The upper atmosphere of Jupiter, *J. Atmos. Sci.* **26**, 826–834, 1969.

Hunten, D. M. and J. Veverka, Stellar and spacecraft occultations by Jupiter: A critical review of derived temperature profiles, in *Jupiter*, T. Gehrels (ed), Univeristy of Arizona Press, pp. 247–283, 1976.

Ingersoll, A. P., The atmosphere of Jupiter, *Space Sci. Rev.* **18**, 603–639, 1976.

Jennings, D. E., V. G. Kunde, F. M. Flasar, M. Abbas, R. Achterberg, P. Ade, A. Barucci, B. Bézard, G. Bjoraker, J. Brasunas, S. Calcutt, R. Carlson, C. Césarsky, B. Conrath, A. Coradini, R. Courtin, A. Coustenis, S. Edberg, C. Ferrari, D. Gautier, P. Gierasch, K. Grossman, and 18 other authors, Infrared measurements of Jupiter from *Cassini* CIRS: Early results, in *Jupiter: Planet, Satellites & Magnetosphere*, Boulder, Colorado, pp. 56–57, 2001.

Kim, S., P. Drossart, J. Caldwell, and J.-P. Maillard, Temperatures of the jovian auroral zone inferred from 2-μm H_2 quadrupole line observations, *Icarus* **84**, 54–61, 1990.

Kim, S. J., J. Caldwell, A. R. Rivolo, R. Wagener, and G. S. Orton, Infrared polar brightening on Jupiter: III. Spectrometry from the *Voyager 1* IRIS experiment, *Icarus* **64**, 233–248, 1985.

Kim, S. J., D. A. Glenar, R. R. Joyce, and T. Kostiuk, Spatial and spectral characteristics of the near-infrared aurorae of Jupiter, *Icarus* **102**, 99–106, 1993.

Kim, Y. H. and J. Fox, The chemistry of hydrocarbon ions in the jovian ionosphere, *Icarus* **112**, 310–325, 1994.

Kim, Y. H., J. L. Fox, and J. J. Caldwell, Temperatures and altitudes of Jupiter's ultraviolet aurora inferred from GHRS observations with the Hubble Space Telescope, *Icarus* **128**, 189–201, 1997.

Kliore, A. J. and P. M. Woiceshyn, Structure of the atmosphere of Jupiter from *Pioneer 10* and *11* radio occultation measurements, in *Jupiter*, T. Gehrels (ed), Univeristy of Arizona Press, pp. 216–237, 1976.

Knyazev, V. D., Á. Bencsura, S. I. Stoliarov, and I. R. Slagle, Kinetics of the $C_2H_3 + H_2 \rightleftharpoons H + C_2H_4$ and $CH_3 + H_2 \rightleftharpoons H + CH_4$ reactions, *J. Phys. Chem.* **100**, 11 346–11 354, 1996.

Kostiuk, T., M. J. Mumma, F. Espenak, D. Deming, D. E. Jennings, W. Maguire, and D. Zipoy, Measurements of stratospheric ethane in the jovian south polar region from infrared heterodyne spectroscopy of the ν_9 band near 12 microns, *ApJ* **265**, 564–569, 1983.

Kostiuk, T., F. Espenak, M. J. Mumma, D. Deming, and D. Zipoy, Variability of ethane on Jupiter, *Icarus* **72**, 394–410, 1987.

Kostiuk, T., F. Espenak, M. J. Mumma, and P. Romani, Infrared studies of hydrocarbons on Jupiter, *Infrared Phys.* **29**, 199–204, 1989.

Kostiuk, T., P. Romani, F. Espenak, T. A. Livengood, and J. J. Goldstein, Temperature and abundances in the jovian auroral stratosphere: 2. Ethylene as a probe of the microbar region, *J. Geophys. Res.* **98**, 18 823–18 830, 1993.

Lagage, P. O., P. Galdemard, E. Pantin, R. Jouan, P. Masse, M. Sauvage, G. Olofsson, M. Huldtgren, L. Nordh, J. A. Belmonte, C. Regulo, J. M. Rodriguez Espinosa, L. Vidal, B. Mosser, A. Ulla, and D. Gautier, Collision of Shoemaker–Levy 9 fragments A, E, H, L, and Q1 with Jupiter: Mid-infrared light curves, *Geophys. Res. Lett.* **22**, 1773–1776, 1995.

Lam, H. A., N. Achilleos, S. Miller, J. Tennyson, L. M. Trafton, T. R. Geballe, and G. E. Ballester, A baseline spectroscopic study of the infrared auroras of Jupiter, *Icarus* **127**, 379–393, 1997.

Landry, B., M. Allen, and Y. L. Yung, Troposphere–stratosphere interactions in a one-dimensional model of jovian photochemistry, *Icarus* **89**, 377–383, 1991.

Lara, L.-M., B. Bézard, C. A. Griffith, J. H. Lacy, and T. Owen, High-resolution 10-micrometer spectroscopy of ammonia and phosphine lines on Jupiter, *Icarus* **131**, 317–333, 1998.

Larson, H. P., U. Fink, and R. R. Treffers, Evidence for CO in Jupiter's atmosphere from airborne spectroscopic observations at 5 microns, *ApJ* **219**, 1084–1092, 1978.

Lee, A. Y. T., Y. L. Yung, and J. Moses, Photochemical mod-

eling of CH_3 abundances in the outer solar system, *J. Geophys. Res.* **105**, 20 207–20 225, 2000.

Lee, Y. T., M. A. Allen, A. J. Friedson, and R. A. West, A 2-D model of C_2H_6 in the jovian stratosphere, *BAAS* **30**, 1067, 1998.

Lellouch, E., Chemistry induced by the impacts: Observations, in *The Collision of Comet Shoemaker–Levy 9 and Jupiter*, K. S. Noll, H. A. Weaver, and P. D. Feldman, eds, pp. 213–242, Cambridge University Press, 1996.

Lellouch, E., B. Bézard, R. Moreno, D. Bockelée-Morvan, P. Colom, J. Crovisier, M. Festou, D. Gautier, A. Marten, and G. Paubert, Carbon monoxide in Jupiter after the impact of Comet Shoemaker–Levy 9, *Planet. Space Sci.* **45**, 1203–1212, 1997.

Lellouch, E., H. Feuchtgruber, T. de Graauw, T. Encrenaz, B. Bézard, M. Griffin, and G. Davis, D/H ratio and oxygen source: A Jupiter-Saturn comparison, in *The Jovian System after Galileo. The Saturnian System before Cassini–Huygens*, pp. 21–22, International Symposium held in Nantes, France, 11–15 May 1998, 1998.

Lellouch, E., B. Bézard, T. Fouchet, H. Feuchtgruber, T. Encrenaz, and T. de Graauw, The deuterium abundance in Jupiter and Saturn from ISO–SWS observations, *A&A* **370**, 610–622, 2001.

Lellouch, E., B. Bézard, J. I. Moses, G. R. Davis, P. Drossart, H. Feuchtgruber, E. A. Bergin, R. Moreno, and T. Encrenaz, The origin of water vapor and carbon dioxide in Jupiter's stratosphere, *Icarus* **159**, 112–131, 2002.

Leovy, C. B., C.-R. Sun, M. H. Hitchman, E. E. Remsberg, J. M. Russell, III, L. L. Gordley, J. C. Gillie, and L. V. Lyjak, Transport of ozone in the middle stratosphere: Evidence for planetary wave breaking, *J. Atmos. Sci.* **42**, 230–244, 1985.

Leovy, C. B., A. J. Friedson, and G. S. Orton, The quasiquadrennial oscillation of Jupiter's equatorial stratosphere, *Nature* **354**, 380–382, 1991.

Levison, H. F., M. J. Duncan, K. Zahnle, M. Holman, and L. Dones, Planetary impact rates from ecliptic comets, *Icarus* **143**, 415–420, 2000.

Li, X. and P. L. Read, A mechanistic model of the quasi-quadrennial oscillation in Jupiter's stratosphere, *Planet. Space Sci.* **48**, 637–669, 2000.

Lindal, G. F., The atmosphere of Neptune: An analysis of radio occultation data acquired with *Voyager 2*, *AJ* **103**, 967–982, 1992.

Lindal, G. F., G. E. Wood, G. S. Levy, J. D. Anderson, D. N. Sweetnam, H. B. Hotz, B. J. Buckles, D. P. Holmes, P. E. Doms, V. R. Eshleman, G. L. Tyler, and T. A. Croft, The atmosphere of Jupiter: An analysis of the *Voyager* radio occultation measurements, *J. Geophys. Res.* **86**, 8721–8727, 1981.

Liu, W. and A. Dalgarno, The ultraviolet spectra of the jovian aurora, *ApJ* **467**, 446–453, 1996a.

Liu, W. and A. Dalgarno, The ultraviolet spectra of the jovian dayglow, *ApJ* **462**, 502–518, 1996b.

Livengood, T. A. and H. W. Moos, Jupiter's north and south polar aurorae with IUE data, *Geophys. Res. Lett.* **17**, 2265–2268, 1990.

Livengood, T. A., D. F. Strobel, and H. W. Moos, Long-term study of longitudinal dependence in primary particle precipitation in the north jovian aurora, *J. Geophys. Res.* **95**, 10 375–10 388, 1990.

Livengood, T. A., T. Kostiuk, F. Espenak, and J. J. Goldstein, Temperature and abundances in the jovian auroral stratosphere: 1. Ethane as a probe of the millibar region, *J. Geophys. Res.* **98**, 18 813–18 822, 1993.

Livengood, T. A., H. U. Käufl, T. Kostiuk, G. L. Bjoraker, P. N. Romani, G. Wiedemann, B. Mosser, and M. Sauvage, Multi-wavelength thermal-infrared imaging of SL–9 impact phenomena, in *Proceedings of the European Shoemaker–Levy 9 Conference, held 13-15 February, 1995*, R. West and H. Böhnhardt, eds, pp. 137–145, no. 52 in ESO Conference and Workshop Proceedings, European Southern Observatory, 1995.

Magalhães, J. A., A. L. Weir, B. J. Conrath, P. J. Gierasch, and S. S. Leroy, Slowly moving thermal features on Jupiter, *Nature* **337**, 444–447, 1989.

Magalhães, J. A., A. L. Weir, B. J. Conrath, P. J. Gierasch, and S. S. Leroy, Zonal motion and structure in Jupiter's upper troposphere from *Voyager* infrared and imaging observations, *Icarus* **88**, 39–72, 1990.

Maguire, W. C., R. E. Samuelson, R. A. Hanel, and V. G. Kunde, Latitudinal variation of acetylene and ethane in the jovian atmosphere from *Voyager* IRIS observations, *BAAS* **16**, 647, 1984.

Mai, H. and K. Jockers, Fabry–Perot imaging of Jupiter's aurora at 2.1 μm, *Icarus* **146**, 494–500, 2000.

Maillard, J.-P., P. Drossart, J. K. G. Watson, S. J. Kim, and J. Caldwell, H_3^+ fundamental band in Jupiter's auroral zones at high resolution from 2400 to 2900 inverse centimeters, *ApJ* **363**, L37–L41, 1990.

Marrero, T. R. and E. A. Mason, Gaseous diffusion coefficients, *J. Phys. Chem. Ref. Data* **1**, 3–118, 1972.

Marten, A., C. de Bergh, T. Owen, D. Gautier, J. P. Maillard, P. Drossart, B. L. Lutz, and G. S. Orton, Four micron high-resolution spectra of Jupiter in the North Equatorial Belt: H_3^+ emissions and the $^{12}C/^{13}C$ ratio, *Planet. Space Sci.* **42**, 391–399, 1994.

McConnell, J. C., B. R. Sandel, and A. L. Broadfoot, *Voyager* UV spectrometer observations of He 584 Å dayglow at Jupiter, *Planet. Space Sci.* **29**, 283–292, 1981.

McGrath, M. A., P. D. Feldman, G. E. Ballester, and H. W. Moos, IUE observations of the jovian dayglow emission, *Geophys. Res. Lett.* **16**, 583–586, 1989.

McIntyre, M. E. and T. N. Palmer, The "surf zone" in the stratosphere, *J. Atmos. Terr. Phys.* **46**, 825–849, 1984.

McNesby, J. R., The photochemistry of Jupiter above 1000 Å, *J. Atmos. Sci.* **26**, 594–599, 1969.

Mordaunt, D. H., I. R. Lambert, G. P. Morley, M. N. R. Ashford, R. N. Dixon, and C. M. Western, Primary product channels in the photodissociation of methane at 121.6 nm, *J. Chem. Phys.* **98**, 2054–2065, 1993.

Moreno, F. and J. Sedano, Radiative balance and dynamics in the stratosphere of Jupiter: Results from a latitude-dependent aerosol heating model, *Icarus* **130**, 36–48, 1997.

Moreno, R., *Observations Millimétriques et Submillimétriques des Planètes Géantes. Etude de Jupiter Après la Chute de la Comète SL9*, Ph.D. thesis, Université Paris-6, 1998.

Morrissey, P. F., P. D. Feldman, M. A. McGrath, B. C. Wolven, and H. W. Moos, The ultraviolet reflectivity of Jupiter at 3.5 Å resolution from *Astro-1* and *Astro-2*, *ApJ* **454**, L65–L68, 1995.

Morrissey, P. F., P. D. Feldman, J. T. Clarke, B. C. Wolven, D. F. Strobel, S. T. Durrance, and J. T. Trauger, Simultaneous spectroscopy and imaging of the jovian aurora with the Hopkins Ultraviolet Telescope and the Hubble Space Telescope, *ApJ* **476**, 918–923, 1997.

Moses, J. I., SL9 impact chemistry: Long-term photochemical evolution, in *The Collision of Comet Shoemaker–Levy 9 and Jupiter*, K. S. Noll, H. A. Weaver, and P. D. Feldman, eds, pp. 243–268, Cambridge University Press, 1996.

Moses, J. I., M. Allen, and G. R. Gladstone, Nitrogen and oxygen photochemistry following SL9, *Geophys. Res. Lett.* **22**, 1601–1604, 1995a.

Moses, J. I., M. Allen, and G. R. Gladstone, Post-SL9 sulfur photochemistry on Jupiter, *Geophys. Res. Lett.* **22**, 1597–1600, 1995b.

Moses, J. I., B. Bézard, E. Lellouch, G. R. Gladstone, H. Feucht-

gruber, and M. Allen, Photochemistry of Saturn's atmosphere. I. Hydrocarbon chemistry and comparisons with ISO observations, *Icarus* **143**, 244–298, 2000a.

Moses, J. I., E. Lellouch, B. Bézard, G. R. Gladstone, H. Feuchtgruber, and M. Allen, Photochemistry of Saturn's atmosphere: II. Effects of an influx of external oxygen, *Icarus* **145**, 166–202, 2000b.

Moses, J. I., T. Fouchet, B. Bézard, E. Lellouch, G. R. Gladstone, H. Feuchtgruber, and M. Allen, Comparative planetology: Lessons from photochemical modeling of the upper atmospheres of Jupiter and Saturn, *BAAS* **33**, 1044, 2001.

Niemann, H. B., S. K. Atreya, G. R. Carignan, T. M. Donahue, J. A. Haberman, D. N. Harpold, R. E. Hartle, D. M. Hunten, W. T. Kasprzak, P. R. Mahaffy, T. C. Owen, and S. H. Way, The composition of the jovian atmosphere as determined by the *Galileo* Probe Mass Spectrometer, *J. Geophys. Res.* **103**, 22 831–22 845, 1998.

Nixon, C. A., D. J. Jennings, P. G. J. Irwin, P. D. Parrish, T. Fouchet, R. K. Achterberg, A. A. Simon-Miller, and the *Cassini* CIRS team, Acetylene and ethane distributions in the jovian stratosphere from *Cassini* CIRS observations, *BAAS* **33**, 1026, 2001.

Noll, K. S. and R. F. Knacke, Response to comment on "Carbon monoxide in Jupiter after Comet Shoemaker–Levy 9," *Icarus* **133**, 322–324, 1998.

Noll, K. S., R. F. Knacke, A. T. Tokunaga, J. H. Lacy, S. Beck, and E. Serabyn, The abundances of ethane and acetylene in the atmospheres of Jupiter and Saturn, *Icarus* **65**, 257–263, 1986.

Noll, K. S., R. F. Knacke, T. R. Geballe, and A. T. Tokunaga, The origin and vertical distribution of carbon monoxide on Jupiter, *ApJ* **324**, 1210–1218, 1988.

Noll, K. S., D. Gilmore, R. F. Knacke, M. Womack, C. A. Griffith, and G. Orton, Carbon monoxide in Jupiter after Comet Shoemaker–Levy 9, *Icarus* **126**, 324–335, 1997.

Ohring, G., The temperature and ammonia profiles in the jovian atmosphere from inversion of the jovian emission spectrum, *ApJ* **184**, 1027–1040, 1973.

Ollivier, J. L., M. Dobrijévic, and J. P. Parisot, New photochemical model of Saturn's atmosphere, *Planet. Space Sci.* **48**, 699–716, 2000.

Orton, G., M. A'Hearn, K. Baines, D. Deming, T. Dowling, J. Goguen, C. Griffith, H. Hammel, W. Hoffmann, D. Hunten, D. Jewitt, T. Kostiuk, S. Miller, K. Noll, K. Zahnle, N. Achilleos, A. Dayal, L. Deutsch, F. Espenak, P. Esterle, J. Friedson, K. Fast, J. Harrington, J. Hora, R. Joseph, D. Kelly, R. Knacke, J. Lacy, C. Lisse, J. Rayner, A. Sprague, M. Shure, K. Wells, P. Yanamandra-Fisher, D. Zipoy, G. Bjoraker, D. Buhl, W. Golisch, D. Griep, C. Kaminski, C. Arden, A. Chaikin, J. Goldstein, D. Gilmore, G. Fazio, T. Kanamori, H. Lam, T. Livengood, M.-M. MacLow, M. Marley, T. Momary, D. Robertson, P. Romani, J. Spitale, M. Sykes, J. Tennyson, D. Wellnitz, and S. W. Ying, Collision of Comet Shoemaker-Levy 9 with Jupiter observed by the NASA Infrared Telescope Facility, *Science* **267**, 1277–1282, 1995.

Orton, G., B. Fisher, L. Barnard, S. Edberg, T. Martin, L. Spilker, L. Tamppari, E. Ustinov, J. Harrington, B. Conrath, P. Gierasch, D. Deming, F. M. Flasar, V. Kunde, R. Achterberg, G. Bjoraker, J. Brasunas, R. Carlson, D. Jennings, C. Nixon, J. Pearl, P. Romani, R. Samuelson, A. Simon-Miller, M. Smith, M. Abbas, P. Ade, A. Barucci, B. Bezard, R. Courtin, A. Coustenis, D. Gautier, E. Lellouch, A. Marten, S. Calcutt, P. Irwin, P. Read, F. Taylor, T. Owen, C. Cesarsky, C. Ferrari, J. P. Meyer, L. Travis, A. Coradini, R. Prangé, K. Grossman, and J. Spencer, Joint *Cassini*, *Galileo* and ground-based infrared observations of Jupiter's atmosphere, *BAAS* **33**, 1035–1036, 2001.

Orton, G. S., The thermal structure of Jupiter: I. Implications of *Pioneer 10* infrared radiometer data, *Icarus* **26**, 125–141, 1975a.

Orton, G. S., The thermal structure of Jupiter: II. Observations and analysis of 8–14 micron radiation, *Icarus* **26**, 142–158, 1975b.

Orton, G. S., Recovery of the mean jovian temperature structure from inversion of spectrally resolved thermal radiance data, *Icarus* **32**, 41–57, 1977.

Orton, G. S. and H. H. Aumann, The abundance of acetylene in the atmosphere of Jupiter, *Icarus* **32**, 431–436, 1977.

Orton, G. S. and A. P. Ingersoll, *Pioneer 10* and *11* and ground-based infrared data on Jupiter: The thermal structure and He–H_2 ratio, in *Jupiter*, T. Gehrels (ed), Univeristy of Arizona Press, pp. 206–215, 1976.

Orton, G. S., A. J. Friedson, J. Caldwell, H. B. Hammel, K. H. Baines, J. T. Bergstralh, T. Z. Martin, M. E. Malcom, R. A. West, W. F. Golisch, D. M. Griep, C. D. Kaminski, A. T. Tokunaga, R. Baron, and M. Shure, Thermal maps of Jupiter: Spatial organization and time dependence of stratospheric temperatures, 1980–1990, *Science* **252**, 537–542, 1991.

Orton, G. S., B. M. Fisher, K. H. Baines, S. T. Stewart, A. J. Friedson, J. L. Ortiz, M. Marinova, M. Ressler, A. Dayal, W. Hoffmann, J. Hora, S. Hinkley, V. Krishnan, M. Masanovic, J. Tesic, A. Tziolas, and K. Parija, Characteristics of the *Galileo* probe entry site from Earth-based remote sensing observations, *J. Geophys. Res.* **103**, 22 791–22 814, 1998.

Owen, T., J. Caldwell, A. R. Rivolo, V. Moore, A. L. Lane, C. Sagan, G. Hunt, and C. Ponnamperuma, Observations of the spectrum of Jupiter from 1500 to 2000 Å with the IUE, *ApJ* **236**, L39–L42, 1980.

Parkinson, C. D., L. Ben Jaffel, and J. C. McConnell, Deuterium abundance from HD and CH_3D reservoirs in the atmosphere of Jupiter, *BAAS* **33**, 1042, 2001.

Perry, J. J., Y. H. Kim, J. L. Fox, and H. S. Porter, Chemistry of the jovian auroral ionosphere, *J. Geophys. Res.* **104**, 16 541–16 565, 1999.

Prangé, R., Jovian UV aurorae, IR aurorae, and particle precipitations: A common origin?, *A&A* **251**, L15–L18, 1991.

Prasad, S. S., L. A. Capone, and L. J. Schneck, Photochemistry of hydrocarbons in the jovian upper atmosphere, *Geophys. Res. Lett.* **2**, 161–164, 1975.

Prather, M. J., J. A. Logan, and M. B. McElroy, Carbon monoxide in Jupiter's upper atmosphere: An extraplanetary source, *ApJ* **223**, 1072–1081, 1978.

Pryor, W. R. and C. W. Hord, A study of photopolarimeter system UV absorption data on Jupiter, Saturn, Uranus, and Neptune: Implications for auroral haze formation, *Icarus* **91**, 161–172, 1991.

Rages, K. and Beebe, R. and Senske, D., Jovian stratospheric hazes: The high phase angle view from *Galileo*, *Icarus* **139**, 211–226, 1999.

Raynaud, E., P. Drossart, K. Matcheva, B. Sicardy, W. Hubbard, F. Roques, T. Widemann, G. Gladstone, J. Waite, P. Bastien, R. Doyon, D. Nadeau, R. Hill, M. Reike, and M. Marley, The 10 October 1999 HIP 9369 occultation by the northern polar region of Jupiter: Ingress and egress lightcurves analysis, *Icarus* **162**, 344–361, 2003.

Ridgway, S. T., Jupiter: Identification of ethane and acetylene, *ApJ* **187**, L41–L43; erratum **192**, L51, 1974.

Ridgway, S. T., H. P. Larson, and U. Fink, The infrared spectrum of Jupiter, in *Jupiter*, T. Gehrels (ed), Univeristy of Arizona Press, pp. 384–417, 1976.

Romani, P. N., Recent rate constant and product measurements of the reactions $C_2H_3 + H_2$ and $C_2H_3 + H$: Importance for photochemical modeling of hydrocarbons on Jupiter, *Icarus* **122**, 233–241, 1996.

Sada, P. V., G. L. Bjoraker, D. E. Jennings, G. H. McCabe, and

P. N. Romani, Observations of CH_4, C_2H_6, and C_2H_2 in the stratosphere of Jupiter, *Icarus* **136**, 192–201, 1998.

Sanchez-Lavega, A., J. M. Gómez, J. F. Rojas, J. R. Acaretta, J. Lecacheux, F. Colas, R. Hueso, and J. Arregui, Long-term evolution of Comet SL–9 impact features: July 1994 – September 1996, *Icarus* **131**, 341–357, 1998.

Seiff, A., D. B. Kirk, T. C. D. Knight, R. E. Young, J. D. Mihalov, L. A. Young, F. S. Milos, G. Schubert, R. C. Blanchard, and D. Atkinson, Thermal structure of Jupiter's atmosphere near the edge of a 5-μm hot spot in the North Equatorial Belt, *J. Geophys. Res.* **103**, 22 857–22 889, 1998.

Sinton, W. M., W. W. Macy, and G. S. Orton, Infrared scans of Jupiter, *Icarus* **42**, 86–92, 1980.

Skinner, T. E., M. T. Deland, G. E. Ballester, K. A. Coplin, P. D. Feldman, and H. W. Moos, Temporal variation of the jovian H I Lyman alpha emission (1979–1986), *J. Geophys. Res.* **93**, 29–34, 1988.

Smith, N. S. and F. Raulin, Modeling of methane photolysis in the reducing atmospheres of the outer solar system, *J. Geophys. Res.* **104**, 1873–1876, 1999.

Smith, P. L., K. Yoshino, W. H. Parkinson, K. Ito, and G. Stark, High-resolution, VUV (147-201 nm) photoabsorption cross sections for C_2H_2 at 195 and 295 K, *J. Geophys. Res.* **96**, 17 529–17 533, 1991.

Spinrad, H. and L. M. Trafton, High dispersion spectra of the outer planets: I. Jupiter in the visual and red, *Icarus* **2**, 19–28, 1963.

Stecher, T. P., The reflectivity of Jupiter in the ultraviolet, *ApJ* **142**, 1186–1190, 1965.

Strobel, D. F., The photochemistry of methane in the jovian atmosphere, *J. Atmos. Sci.* **26**, 906–911, 1969.

Strobel, D. F., The photochemistry of hydrocarbons in the jovian atmosphere, *J. Atmos. Sci.* **30**, 489–498, 1973.

Strobel, D. F., Hydrocarbons abundances in the jovian atmosphere, *ApJ* **192**, L47–L49, 1974.

Strobel, D. F., Aeronomy of the major planets: Photochemistry of ammonia and hydrocarbons, *Rev. Geophys. Space Phys.* **13**, 372–382, 1975.

Strobel, D. F., Photochemistry of the reducing atmospheres of Jupiter, Saturn and Titan, *Int. Rev. Phys. Chem.* **3**, 145–176, 1983.

Strobel, D. F. and Y. L. Yung, The Galilean satellites as a source of CO in the jovian upper atmosphere, *Icarus* **37**, 256–263, 1979.

Tokunaga, A., R. F. Knacke, and T. Owen, Ethane and acetylene abundances in the jovian atmosphere, *ApJ* **209**, 294–301, 1976.

Tokunaga, A. T., S. C. Beck, T. R. Geballe, J. H. Lacy, and E. Serabyn, The detection of HCN on Jupiter, *Icarus* **48**, 283–289, 1981.

Tomasko, M. G., E. Karkoschka, and S. Martinek, Observations of the limb darkening of Jupiter at ultraviolet wavelengths and constraints on the properties and distribution of stratospheric aerosols, *Icarus* **75**, 381–398, 1986.

Trafton, L. M., Model atmospheres of the major planets, *ApJ* **147**, 765–781, 1967.

Trafton, L. M., J. C. Gérard, G. Munhoven, and J. H. Waite, Jr., High-resolution spectra of Jupiter's northern auroral ultraviolet emission with the Hubble Space Telescope, *ApJ* **421**, 816–827, 1994.

Vervack, Jr., L. M., B. R. Sandel, G. R. Gladstone, J. C. McConnell, and C. D. Parkinson, Jupiter's He 584 Å dayglow: New results, *Icarus* **114**, 163–173, 1995.

von Zahn, U., D. M. Hunten, and G. Lehmacher, Helium in Jupiter's atmosphere: Results from the *Galileo* probe Helium Interferometer Experiment, *J. Geophys. Res.* **103**, 22 815–22 829, 1998.

Wagener, R., J. Caldwell, T. Owen, S.-J. Kim, T. Encrenaz, and M. Combes, The jovian stratosphere in the ultraviolet, *Icarus* **63**, 222–236, 1985.

Waite, Jr., J. H., T. E. Cravens, J. Kozyra, A. F. Nagy, S. K. Atreya, and R. H. Chen, Electron precipitation and related aeronomy of the jovian thermosphere and ionosphere, *J. Geophys. Res.* **88**, 6143–6163, 1983.

Wallace, L., The thermal structure of Jupiter in the stratosphere and upper troposphere, in *Jupiter*, T. Gehrels (ed), Univeristy of Arizona Press, pp. 284–303, 1976.

Wallace, L. and D. M. Hunten, The Lyman-alpha albedo of Jupiter, *ApJ* **73**, 1013–1031, 1973.

Wallace, L. and G. R. Smith, On jovian temperature profiles obtained by inverting thermal spectra, *ApJ* **203**, 760–763, 1976.

Wallace, L., M. Prather, and M. J. S. Belton, The thermal structure of the atmosphere of Jupiter, *ApJ* **193**, 481–493, 1974.

Wang, J.-H., K. Liu, Z. Min, H. Su, R. Bersohn, J. Preses, and J. Z. Larese, Vacuum ultraviolet photochemistry of CH_4 and isotopomers: II. Product channel fields and absorption spectra, *J. Chem. Phys.* **113**, 4146–4152, 2000.

West, R. A., *Voyager 2* imaging eclipse observations of the jovian high altitude haze, *Icarus* **75**, 381–398, 1988.

West, R. A., Particles in Jupiter's atmosphere from the impacts of Comet P/Shoemaker–Levy 9, in *The Collision of Comet Shoemaker–Levy 9 and Jupiter*, K. S. Noll, H. A. Weaver, and P. D. Feldman, eds, pp. 269–292, Cambridge University Press, 1996.

West, R. A., D. F. Strobel, and M. G. Tomasko, Clouds, aerosols, and photochemistry in the jovian atmosphere, *Icarus* **65**, 161–217, 1986.

West, R. A., A. J. Friedson, and J. F. Appleby, Jovian large-scale stratospheric circulation, *Icarus* **100**, 245–259; erratum **130**, 557, 1992.

Wildt, R., Absorptionsspektren und atmosphären der grossen planeten, *Nachr. Ges. Akad. Wiss. Göttigen* **1**, 87–96, 1932.

Wildt, R., Photochemistry of planetary atmospheres, *ApJ* **86**, 321–336, 1937.

Wilson, E. H. and S. K. Atreya, Benzene formation in the atmosphere of Titan, *BAAS* **32**, 1025, 2000.

Wong, A.-S., A. Y. T. Lee, Y. L. Yung, and J. M. Ajello, Jupiter: Aerosol chemistry in the polar atmosphere, *ApJ* **534**, L215–L217, 2000.

Wong, A.-S., Y. L. Yung, and A. J. Friedson, Benzene and haze formation in the polar atmosphere of Jupiter, *Geophys. Res. Lett.* **30**, 30–1, 2003.

Yelle, R. V., L. A. Young, R. J. Vervack, Jr., R. Young, L. Pfister, and B. R. Sandel, Structure of Jupiter's upper atmosphere: Predictions for *Galileo*, *J. Geophys. Res.* **101**, 2149–2161, 1996.

Yelle, R. V., C. A. Griffith, and L. A. Young, Structure of the jovian stratosphere at the *Galileo* probe entry site, *Icarus* **152**, 331–346, 2001.

Yung, Y. L. and W. B. DeMore, *Photochemistry of Planetary Atmospheres*, Oxford University Press, 1999.

Yung, Y. L. and D. F. Strobel, Hydrocarbon photochemistry and Lyman alpha albedo of Jupiter, *ApJ* **239**, 395–402, 1980.

Yung, Y. L., G. R. Gladstone, K. M. Chang, J. M. Ajello, and S. K. Srivastava, H_2 fluorescence spectrum from 1200 to 1700 Å by electron impact: Laboratory study and application to jovian aurora, *ApJ* **254**, L65–L69, 1982.

Yung, Y. L., M. Allen, and J. P. Pinto, Photochemistry of the atmosphere of Titan: Comparison between model and observations, *Astrophys. J. Suppl. Ser.* **55**, 465–506, 1984.

Zahnle, K., Dynamics and chemistry of SL9 plumes, in *The Collision of Comet Shoemaker–Levy 9 and Jupiter*, K. S. Noll, H. A. Weaver, and P. D. Feldman, eds, pp. 183–212, Cambridge University Press, 1996.